การพัฒนาพอลิไอไมด์/พอลิซัลโฟนคอมโพสิตนำไฟฟ้าในวัสดุที่มีสัมประสิทธิ์ความต้านทานไฟฟ้าตาม
อุณหภูมิเชิงบวก

นายนพวัต กิ่งพุทธพงศ์

วิทยานิพนธ์นี้เป็นส่วนหนึ่งของการศึกษาตามหลักสูตรปริญญาวิศวกรรมศาสตรมหาบัณฑิต
สาขาวิชาวิศวกรรมเคมี ภาควิชาวิศวกรรมเคมี
คณะวิศวกรรมศาสตร์ จุฬาลงกรณ์มหาวิทยาลัย
ปีการศึกษา 2560

DEVELOPMENT OF CONDUCTIVE POLYIMIDE/POLYSULFONE COMPOSITES AS POSITIVE TEMPERATURE COEFFICIENT MATERIALS

Mr. Noppawat Kuengputpong

A Thesis Submitted in Partial Fulfillment of the Requirements
for the Degree of Master of Engineering Program in Chemical Engineering
Department of Chemical Engineering
Faculty of Engineering
Chulalongkorn University
Academic Year 2017

Thesis Title	DEVELOPMENT OF CONDUCTIVE POLYIMIDE/POLYSULFONE COMPOSITES AS POSITIVE TEMPERATURE COEFFICIENT MATERIALS
By	Mr. Noppawat Kuengputpong
Field of Study	Chemical Engineering
Thesis Advisor	Professor Sarawut Rimdusit, Ph.D.
Thesis Co-Advisor	Assistant Professor Sunan Tiptipakorn, D.Eng.

Accepted by the Faculty of Engineering, Chulalongkorn University in Partial Fulfillment of the Requirements for the Master's Degree

.....Dean of the Faculty of Engineering

(Associate Professor Supot Teachavorasinskun, Ph.D.)

THESIS COMMITTEE

.....Chairman

(Professor Siriporn Damrongsakkul, Ph.D.)

.....Thesis Advisor

(Professor Sarawut Rimdusit, Ph.D.)

.....Thesis Co-Advisor

(Assistant Professor Sunan Tiptipakorn, D.Eng.)

.....Examiner

(Chalida Klaysom, Ph.D.)

.....External Examiner

(Passarin Jongvisuttisun, Ph.D.)

นพวัต กิ่งพุทธพงศ์ : การพัฒนาพอลิไอไมด์/พอลิซัลโฟนคอมโพสิตนำไฟฟ้าในวัสดุที่มีสัมประสิทธิ์ความต้านทานไฟฟ้าตามอุณหภูมิเชิงบวก (DEVELOPMENT OF CONDUCTIVE POLYIMIDE/POLYSULFONE COMPOSITES AS POSITIVE TEMPERATURE COEFFICIENT MATERIALS) อ.ที่ปรึกษาวิทยานิพนธ์หลัก: ศ. ดร. ศราวุธ ริมดุสิต, อ.ที่ปรึกษาวิทยานิพนธ์ร่วม: ผศ. ดร. สุนันท์ ทิพย์ทิพากร, 85 หน้า.

การทำคอมโพสิตนำไฟฟ้าในวัสดุที่มีสัมประสิทธิ์ความต้านทานไฟฟ้าตามอุณหภูมิเชิงบวกจะต้องมีค่าความต้านทานเชิงปริมาตรที่อุณหภูมิห้องต่ำกว่า 10^4 โอห์ม•เซนติเมตร การทำให้วัสดุพอลิไอไมด์ที่มีสัมประสิทธิ์ความต้านทานไฟฟ้าตามอุณหภูมิเชิงบวกมีสภาพนำไฟฟ้าอยู่ในช่วงดังกล่าวสามารถทำได้โดยการใช้คาร์บอนแบล็คเป็นสารตัวเติมนำไฟฟ้า สำหรับการทำให้วัสดุที่มีสัมประสิทธิ์ความต้านทานไฟฟ้าตามอุณหภูมิเชิงบวกมีช่วงการเปลี่ยนแปลงค่าความต้านทานไฟฟ้านั้น วิธีที่ได้รับความนิยมคือการนำพอลิเมอร์อีกชนิดเข้ามาผสมเข้ากับพอลิไอไมด์ นอกจากนี้วิธีนี้ยังช่วยลดปริมาณการเติมคาร์บอนแบล็คในคอมพอสิตนำไฟฟ้าได้อีกด้วย โดยมีลักษณะการผสมที่เข้ากันได้บางส่วน และทำให้คาร์บอนแบล็คกระจายตัวอยู่ในส่วนวัฏภาคใดวัฏภาคหนึ่งของพอลิเมอร์ที่ผสมเข้ากันได้บางส่วน ซึ่งจะทำให้เกิดปรากฏการณ์ดับเบิลเพอร์โคเลชัน (Double percolation) ที่ช่วยลดปริมาณการเติมคาร์บอนแบล็คให้น้อยลงมากที่สุด และเมื่อให้ความร้อนแก่ชิ้นงาน จนถึงอุณหภูมิเปลี่ยนสถานะคล้ายแก้วของชิ้นงานจะเกิดปรากฏการณ์การเปลี่ยนแปลงความต้านทานไฟฟ้าจากสภาพนำไฟฟ้าเป็นสภาพฉนวน ในงานวิจัยนี้คอมโพสิตนำไฟฟ้าในวัสดุที่มีสัมประสิทธิ์ความต้านทานไฟฟ้าตามอุณหภูมิเชิงบวกเตรียมขึ้นจากการผสมพอลิเมอร์ระหว่างพอลิไอไมด์กับพอลิซัลโฟน ที่อัตราส่วน 100/0 ถึง 10/90 โดยน้ำหนัก โดยใช้คาร์บอนแบล็คเป็นสารตัวเติมนำไฟฟ้าในปริมาณ 0-20 เปอร์เซ็นต์โดยน้ำหนัก และเป็นพอลิเมอร์สมบูรณ์ที่อุณหภูมิ 300 องศาเซลเซียส จากการศึกษาพบว่าพอลิเมอร์ผสมระหว่างพอลิไอไมด์กับพอลิซัลโฟนมีพฤติกรรมเป็นพอลิเมอร์ผสมที่สามารถผสมเข้ากันได้บางส่วน และสามารถช่วยลดช่วง เพอร์โคเลชันเทรชโฮลด์ (Percolation threshold) ให้มีค่าต่ำลง และเพิ่มค่าการนำไฟฟ้าดีกว่าการใช้พอลิไอไมด์เพียงชนิดเดียว เมื่อพิจารณาค่าความต้านทานไฟฟ้าของคอมโพสิตที่เกิดจากพอลิเมอร์ผสม พบว่า สามารถลดปริมาณการเติมคาร์บอนแบล็คได้ถึง 90 เปอร์เซ็นต์ เมื่อเปรียบเทียบกับการใช้พอลิไอไมด์ชนิดเดียว และเมื่อพิจารณาค่าความต้านทานไฟฟ้าของคอมโพสิตต่ออุณหภูมิที่เปลี่ยนแปลงไป พบว่า มีพฤติกรรมเป็นแบบวัสดุที่มีสัมประสิทธิ์ความต้านทานไฟฟ้าตามอุณหภูมิเชิงบวกที่ช่วงอุณหภูมิ 180 ถึง 200 องศาเซลเซียส ผลการตรวจสอบการกระจายตัวของอนุภาคนำไฟฟ้าด้วยกล้องจุลทรรศน์ พบว่า อนุภาคนำไฟฟ้ามีการกระจายตัวบริเวณพอลิไอไมด์ดีกว่าในพอลิซัลโฟน นอกจากนั้นสมบัติการรับแรงดึงและเสถียรภาพทางความร้อนของคอมโพสิตนำไฟฟ้าพบว่าผ่านตามเกณฑ์มาตรฐาน ซึ่งแสดงให้เห็นถึงศักยภาพของการใช้เป็นวัสดุที่มีสัมประสิทธิ์ความต้านทานไฟฟ้าตามอุณหภูมิเชิงบวกสำหรับอุปกรณ์อิเลคทรอนิกส์ได้

ภาควิชา วิศวกรรมเคมี	ลายมือชื่อนิสิต .....
สาขาวิชา วิศวกรรมเคมี	ลายมือชื่อ อ.ที่ปรึกษาหลัก .....
ปีการศึกษา 2560	ลายมือชื่อ อ.ที่ปรึกษาร่วม .....

5970208021 : MAJOR CHEMICAL ENGINEERING
KEYWORDS: POSITIVE TEMPERATURE COEFFICIENT / CONDUCTIVE POLYMER COMPOSITE / CARBON BLACK / PERCOLATION THRESHOLD / ELECTRICAL PROPERTIES

NOPPAWAT KUENGPUTPONG: DEVELOPMENT OF CONDUCTIVE POLYIMIDE/POLYSULFONE COMPOSITES AS POSITIVE TEMPERATURE COEFFICIENT MATERIALS. ADVISOR: PROF. SARAWUT RIMDUSIT, Ph.D., CO-ADVISOR: ASST. PROF. SUNAN TIPTIPAKORN, D.Eng., 85 pp.

For positive temperature coefficient (PTC) applications of electrically conductive composites, volume resistivity at room temperature of lower than 10^4 Ω.cm is one major requirement. Conductive polyimide (PI) PTC with the above level of conductivity value can be achieved by a use of carbon black (CB) as conductive filler. For materials with PTC, there is a change in resistance related to temperature. In order to reduce the amount of CB used in the PTC composites, one of well-known methods is to introduce another polymer into a polymer to generate immiscible blends. When the conductive filler is dispersed in one polymer phase, a system of double percolation with minimal filler content can be achieved. When heating the conductive composite beyond the glass transition temperature, the conductive state of the system changes to insulated state. In this research, conductive composites in materials with PTC are prepared by polymerization between PI and polysulfone (PSF) at a ratio of 100/0 to 10/90 by weight, using CB with loading from 0 to 20% by weight. From the study, it is found that polymer blends between PI/PSF behaved as partially miscible in nature. The blends evidently provided a reduced percolation threshold by 90% with the obtained greater electrical conductivity values than those of the CB-filled PI composites. Considering the volume resistivity of the conductive composite with the change in temperature, it is found that the behavior is PTC material at a temperature range of 180 to 200 °C. Optical microscopic has been used to verify the preferential location of the conductive CB particles in PI domains rather than in the PSF domains. Moreover, the obtained tensile and thermal properties of conductive composites were also found to provide the values meet those standards. The results, therefore, revealed the potential to apply the obtained PTC composites in electronic applications.

Department:	Chemical Engineering	Student's Signature	.....
Field of Study:	Chemical Engineering	Advisor's Signature	.....
Academic Year:	2017	Co-Advisor's Signature	.....

ACKNOWLEDGEMENTS

I would like to express my deep appreciation and sincerest gratitude to my advisor, Prof. Dr. Sarawut Rimdusit and my co-advisor, Assist. Prof. Dr. Sunan Tiptipakorn with their kindness, invaluable supervision, guidance, advice, and encouragement throughout the course of this study. In addition, I would like to thank Assoc. Prof Dr. Siriporn Damrongsakkul as the chairperson, Dr. Chalida Klaysom, and Dr. Passarin Jongvisuttisun for their invaluable comments as a thesis committee.

The authors would like to thank Department of Electrical Engineering, Chulalongkorn University for electrical resistivity measurement and positive temperature coefficient behavior.

Additionally, I would like to thank a members of Polymer Engineering Laboratory of the Department of Chemical Engineering, Faculty of Engineering Chulalongkorn University, for their friendly encouragement, discussion, and assistance in solving problems. Finally, my deepest regards to my family, especially my parents, who have always been the source of my generous encouragement, and unconditional love during my studies. Also, every person who deserves thanks for support and encouragement that cannot be listed.

CONTENTS

Page

Page

Page

LIST OF TABLES

LIST OF FIGURES

CHAPTER I
INTRODUCTION

1.1 Overview

Currently, conductive materials have attracted more and more attention in various areas, such as electro-chromic display, electromagnetic interference shielding, photovoltaic conversion and conductive layer [1-4]. Compared with traditional metal conductive materials, polymer-based conductive materials have increasing popularity in recent years because of their light weight, resistance to corrosion, flexibility, and processing advantages [5-8]. In the developed fields of polymer-based conductive materials, super-engineering plastics are of great interest. They are sought as an alternative for metals in the field of aerospace technology and energy industry because of their outstanding properties [9-12].

The using of electrical conductive polymers or electrical conductive composites depend on the resistivity for the using as electrical conductor, which has surface resistivity in a range of 10^1 to 10^6 Ω/square or volume resistivity in a range of 10^1 to 10^4 Ω.cm. Electrical conductive polymers are electrical conductivity that is not permanent but electrical conductive composites are a permanent electrical conductivity properties. Electrical conductive polymers are widely used as, sensor and switch in antistatic plastic film, printed circuit board, conductive adhesive, polymer light emitting diode (PLED), transparent conductive electrode (TCE), and positive temperature coefficient (PTC) [13].

Positive temperature coefficient materials are primarily designed for the protection of wound equipment such as transformers and motors. The resistance of the PTC materials is low and relatively constant at low temperatures. As the ambient

temperature increases, the resistance rises. The rate of increase becomes very rapid at the reference temperature (T_R) [14].

Generally, polysulfone (PSF) is used in different applications such as medical and food-processing equipment, electrical and electronic components, camera cases, and piping [15]. According to many researches, inorganic fillers, zeolites and ceramics, are used to prepare composite films and membranes due to their ability to be exfoliated in polymeric matrices at a nanoscale level. PSF has attracted attention for many applications, and the most interesting processes using polysulfone are gas separation and membranes in fuel cell [16].

Nowadays, polyimides are attractive polymers due to their outstanding properties such as thermal-oxidative stability, high glass transition temperature, good resistance to solvents, and the mechanical properties. Because of these reasons, they are widely applied in electrical and electronic applications. Furthermore, they have been used as polymeric components of hybrid organic–inorganic (O–I) systems by the sol–gel route. O–I hybrid systems are a meaningful class of new materials, where put together, all useful properties of a ceramic phase (heat resistance, retention of mechanical properties at high temperatures and low thermal expansion) and those of organic polymers (toughness, ductility and process ability) are produced [17].

The addition of conductive fillers in polymer blends has been widely used in the industry because of the electrically insulative properties of almost polymer. The conductive fillers i.e. carbon black (CB), carbon fiber (CF), carbon nanotube (CNT), graphite, metal particle, etc. CB is used generally due to low cost. Furthermore, carbon black is used to enhance the mechanical and electrical properties [18]. Addition of CB powder into plastics is satisfactory because CB tends to form network structure by which desired conductivity in a range of 10^1 to 10^6 Ω/square and 10^1 to 10^4 Ω.cm [19].

For many simple binary systems the percolation threshold is 12-15 vol% filler [20], although it can be greatly lower or higher [21] depending on the conductivity level required. Lowering this percolation threshold performs to be an effective way of reducing the required amount of conductive filler and hence the processing-related problems, while keeping the all-important conductivity at sufficient levels and minimizing issues arising from mechanical properties. Nevertheless, for binary systems (i.e. carbon black mixed with one polymer) there is a direct and intrinsic coupling between the electrical percolation, which gives the mechanical percolation, and a low conductivity, which reduced processing ability. Alternatively, partially miscible blends or binary immiscible can be plan in a technique which prefer the dispersion of CB particles in the minor component of co-continuous blends [22].

Several studies [21-28] have shown that the selective localization of conducting particles in one of the phases or at best at the interface of co-continuous two-phase polymer blend is very effective strategy to decrease the CB percolation threshold. Such systems in which conductive fillers form connective network within one phase or at interface of co-continuous blends can be defined as double percolation or percolation in percolation. According to percolation theory, double percolation or connectivity of filler within the connective phase gives rise to the reduced critical concentration or percolation threshold of the filler [19]. Consequently, reducing CB loading in conductive polymer composites is a major research challenge.

The purpose of this research is to determine the effect of CB on electrical, mechanical and thermal properties of the resulting conductive polyimide composites for positive temperature coefficient materials. The obtained polyimide composite will also be compared with commercial conductive polyimide.

1.2 Objectives

1. To investigate effects of blend composition on PI/PSF morphology.
2. To systematically investigate the effects of carbon black content on electrical, mechanical and thermal properties of conductive PI/PSF composites as a positive temperature coefficient materials

1.3 Scope of the Study

1. Preparing PI/PSF blends and PI/PSF/CB composites via solution casting method.

2. Determining the optimum content of PSF in PI/PSF blends by varying PSF content from 0 to 90 wt%.

3. Preparing conductive PI/PSF composite by using carbon black as conductive filler from 0 to 20 wt%.

4. Investigating the properties of conductive PI/PSF composites as followed:

Physical properties

- Specific gravity
- Viscosity (Viscometer)
- Morphology (OM or SEM)
- Resistivity (Electrometer)

Mechanical properties

- Tensile properties (UTM)
- Storage and loss modulus (DMA)

Thermal properties

- Glass transition temperature (DSC or DMA)
- Degradation temperature and char yield (TGA)

5. Characterization of functional groups of PI/PSF composites using Fourier transform infrared spectroscope (FTIR).

6. Investigation of the positive temperature coefficient behaviors of the resulting PI/PSF composites.

1.4 Procedure of the Study

1. Preparation of chemicals, apparatus and equipment for this research.

2. Synthesis of PI from 3,4,3',4'-biphenyltetracarboxylic dianhydride (*s*-BPDA) and 4,4'-oxydianiline (4,4'-ODA).

3. Determination of mixing or processing conditions of the PI, PSF and their blends.

4. Examination of PI/PSF blends by varying compositions of PSF from 0 to 90 wt% and evaluated physical and mechanical properties.

5. Examination conductive PI/PSF/CB composite by using minimization of CB.

6. Evaluation of electrical, mechanical and thermal properties of conductive PI/PSF/CB composites.

7. Analysis of the experimental results.

8. Preparation of the final report.

CHAPTER II
THEORY

2.1 Positive Temperature Coefficient Materials

PTC materials (Figure 2.1) are used instead of conventional fuses to protect loads such as motors, transformers, etc. or electronic circuits against overcurrent. They are not only respond to inadmissibly high currents but also if a preset temperature limit is exceeded. PTC materials limit the power dissipation of the overall circuit by increasing their resistance and thus reducing the current to a harmless residual value. In contrast to conventional fuses, they do not have to be replaced after elimination of the fault but resume their protective function immediately after a short cooling-down time [29].

Figure 2.1: Positive temperature coefficient materials [30].

2.2 Principles of PTC Materials

At room temperature, the PTC materials have conductive pathway which electric current can move to pass in material due to low resistivity. Then, the potential energy of charge transfer is changed to heat which is collected in PTC materials. When

the temperature is increased up to reference temperature of switching temperature (T_R), the conductive pathway of PTC materials are expanded because of heat capacity in material. So, resistivity is increased vary rapid, effects to reducing of electric current move to pass in material [14]. The principle of PTC materials is detailed in Figure 2.2

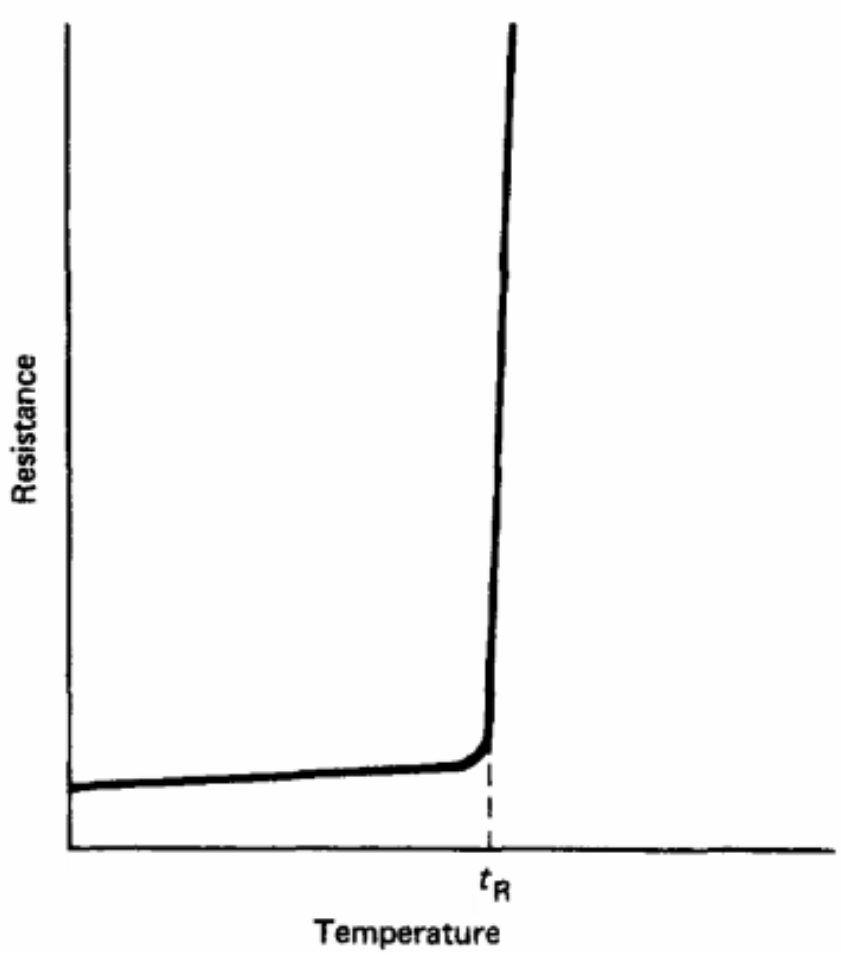

Figure 2.2: Relationship between temperature and resistivity of PTC materials [14, 30].

2.3 Material Configuration

Within a typical PTC materials [29], four distinct classes of materials are used:

- Cable (conductor)
- Protecting tube (insulator)

• Main heater body or PTC chip

- Ceramic (heat capacity)

- Conductive layer (anode and cathode)

A simple typical PTC materials make-up is detailed in Figure 2.3 below.

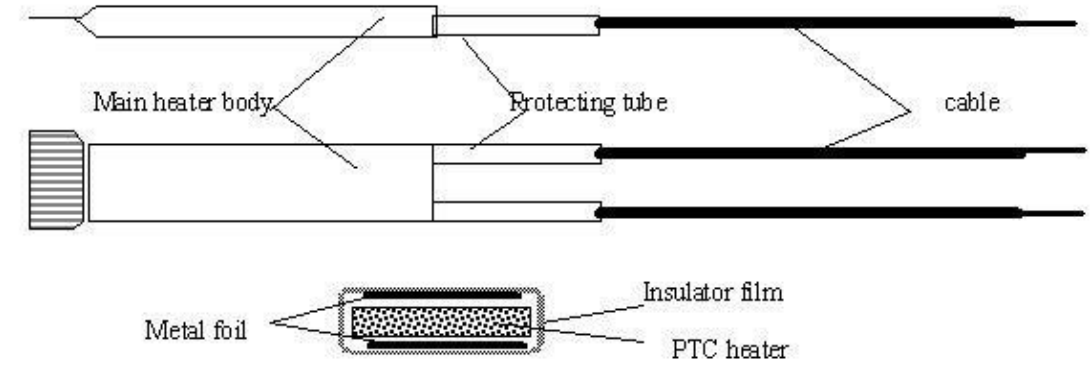

(a)

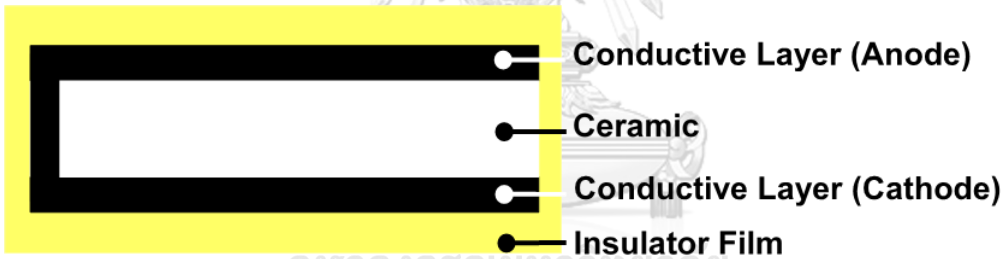

(b)

Figure 2.3: Ingredient of (a) PTC materials, (b) PTC chip [31].

Conductive layer

Conductive layer is a silicone-based or polyimide-based (for high temperature) heat-transfer compound that has a thickness in the range from 10 μm-100 μm [32]. The ability of conductive layer must insulate high thermal which has surface resistivity in a range of 10^1 to 10^6 Ω/square or volume resistivity in a range of 10^1 to 10^4 Ω.cm [19].

Requirement for conductive is presented a range of differing properties (see Table 2.1), which are called upon by circuit designers where their blend of electrical and mechanical performance capabilities and costs best suit the application at hand. As previously discussed, the two materials that receive by far the most attention are polyimide films [33].

Table 2.1: Properties of conductive layer [33].

Property	Conductive Layer
Volume resistivity at room temperature (Ω.cm)	10^1-10^5
Tensile strength (MPa)	35
Tensile modulus (GPa)	2.0-4.0
Yield strain (%)	>2
Elongation at break (%)	>2
Glass transition temperature (T_g, °C)	120 - 200

2.4 Morphology of Polymer Blends

The morphology produced during mixing depends on the interfacial tension between the phases, the blend ratio, the viscosities and relative viscosities, elasticities, and processing condition. Blending of two polymers generally results in the formation of an immiscible heterogeneous two-phase system according to themodynamic principles. Commonly, the morphology of multiphase polymer blends depends on the composition, blending condition, and the rheological properties of the individual components [28]. Several morphologies can be earned over the all composition range. At low contents, the morphology of dispersed phase-matrix is discovered in which the shape of the dispersed phase can be lamella, fibrillar, or spherical depending on the shear history during processing. As the blend ratio raises, a separated phase beings to exude into discontinuous shapes, though still memorable as disperse domains, because of coalescence. Moreover increase in the number of the separated phase will result in phase inversion, before which a co-continuous structure is formed. That is

both phase seem to be continuous throughout the observed filed. Yet higher phase ratios yield an inversion where the dispersed phase becomes the continuous matrix and the matrix phase becomes separated domains.

An example of morphological evolution is shown in the binary images in Figure 2.4, taken from the work of Ravati, S., and Favis, B.D. [34].

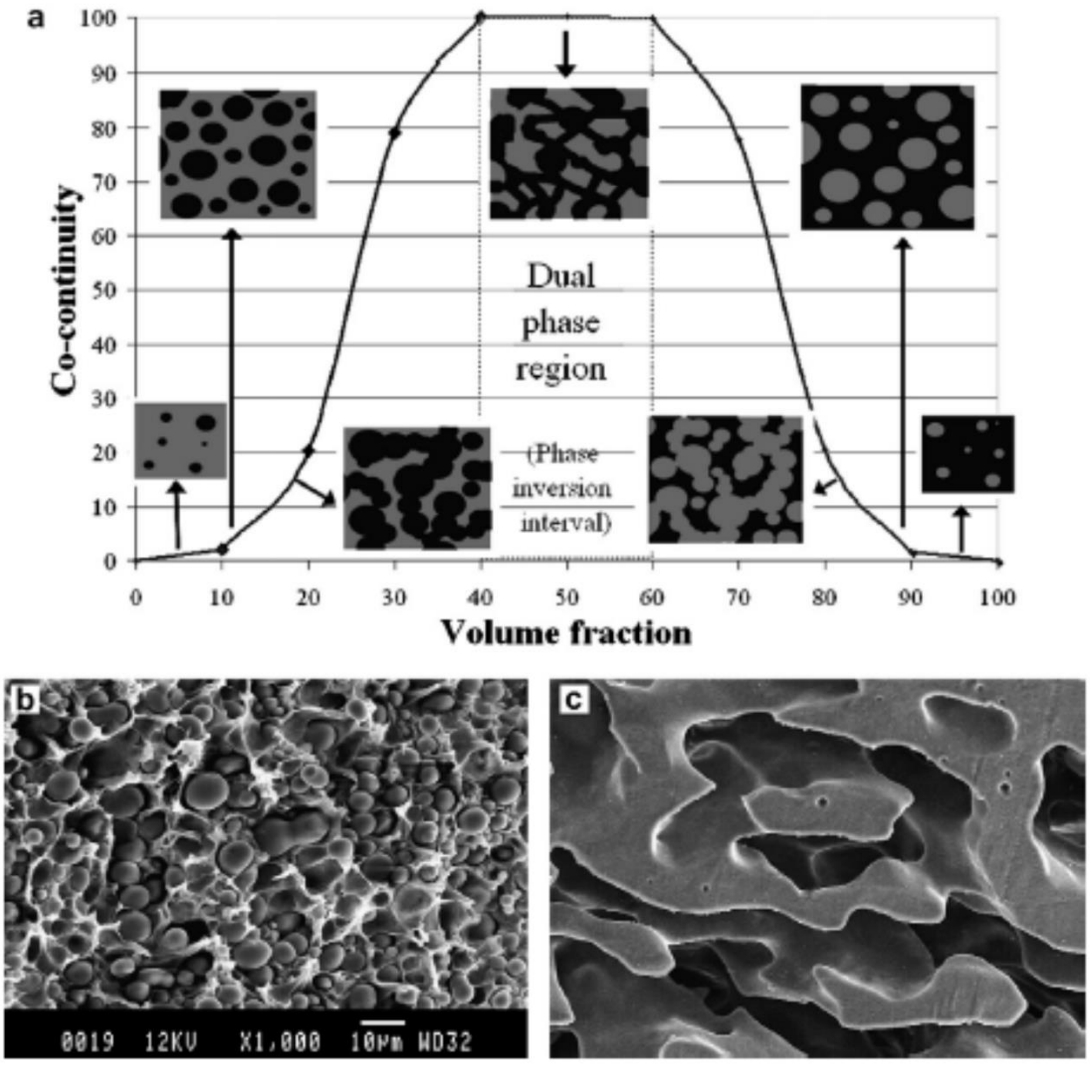

Figure 2.4: (a) Schematic representation of the evolution of morphology in a binary blend, (b) matrix/dispersed morphology and (c) co-continuous morphology [34].

Generally, the morphologies of polymer blends are straight related to the viscoelastic properties of their individual components. The point of phase inversion at

which co-continuity is observed may be related to the rheological appearances of the pure materials through a semi-empirical model [28].

Avgerpoulos et al. [35] used a relationship between the torque ratio and the composition (volume fraction) expressed as:

$$\frac{\tau_1}{\tau_2} = \frac{\phi_1}{\phi_2} \quad (2.1)$$

where τ_i is the torque during mixing in an internal mixer and ϕ_i is the volume fraction of polymer i.

Now, the mechanism of nanoparticle-induced co-continuity is non-finite. In accordance with Paul and Barlow [36], the condition for phase inversion from a separated structure to a co-continuous one is shown as:

$$\frac{\phi_1}{\phi_2} = \frac{\eta_1}{\eta_2} \quad (2.2)$$

Where ϕ_i is the volume fraction, η_1 is melt viscosity, and i indicates phase 1 or 2.

That is an enlargement in the volume fraction or a reducing in the viscosity of the minor polymer would increase its continuity in the matrix. The nanoparticle's selective location will truly provide augmentative volume to the minor polymer. Nevertheless, in the case of the CB-filled PS/PE system, the CB content is too little (about 4 wt%) to decrease the phase reversion point of PE from 40% to 10 wt% [37].

2.5 Carbon Black

Carbon black (CB) is a substance that has ascribed immensely use in an amount of application. It includes mostly of carbon-element, and it is in uniform of spherical particle that have been annealed jointly to aggregate models that are classically around 30-100 nm in size. CB is generally used as a reinforcing filler to improve

dimensional stability, a conductive filler, an ultraviolet light stabilizer, an antioxidant to prolong the lifetime of rubber, and a pigment or colorant. CB is an amorphous form of carbon with a structure comparable to disordered graphite. When aromatic hydrocarbons are subjected to partial combustion at high temperature their molecules will dissociate through the rupture of C H bonds. Afterward, carbon atoms and aromatic radicals react to form layer structures composed of hexagonal carbon rings, which tend to stack in three to four layers, forming crystallographic structures. Crystallites then form primary particles, which further fuse into primary aggregates. Van der Waals forces cause these aggregates to join in more loosely collected agglomerations [13, 38].

There are five types of CBs manufactured in the CB manufacturing: furnace black, thermal black, lampblack, channel black and acetylene black. Different processes form various products with various chemical and physical properties. The most normally used CBs in plastics and rubber applications are thermal and furnace blacks. Over 90% of the CBs immediately produced are made by the furnace process which oil is thermally degraded to form CB particles. Only CBs with large surface area and small diameter are suitable as the filler to enhance electric conductivity [38].

2.5.1 Basic Information on Carbon Black [37, 39]

CB results from thermal cracking or partial combustion of a hydrocarbon raw material (Figure 2.5). Currently almost all CBs are generated by the oil furnace process: a greatly aromatic substrate is incompletely burned by atomization into a hot flame made of preheated air and natural gas, the reactor temperature attainment more than 1500°C. At the process end, pelletized CB or power (“fluffy”) is assembled. The oil furnace process permits effective control of end product chemical and physical properties.

$$C_xH_x + O_2 \xrightarrow{\text{heat}} C + CO + CH_4 + CO_2 + H_2 + H_2O$$

Figure 2.5: Partial oxidation of aromatic hydrocarbons.

CB is a particulate form of industrial carbon at which demonstrates a "quasi-graphitic" microstructure (Figure 2.6). The generating process releases diverse forms of oxygenated groups on carbon black layer planes: mostly carboxyl, quinolic and phenolic chemisorbed complexes. During the nucleation process (Figure 2.7), three to four layers shape crystallites, which mix to shape primary particles and continue to develop into aggregates. Agglomerates are an intense assembly of aggregates established because of the teeny length between them and the strong van der Waal forces appear. The dispersion of CB in a polymer matrix will require the destroying of these links. An aggregate is represents and inseparable the CB "base unit" albeit a CB is often characterized by its primary particle size. In summary, the finer the prime particles, and subsequently the smaller the aggregates, the lower will be the level of electrical resistivity when separated in polymer matrix.

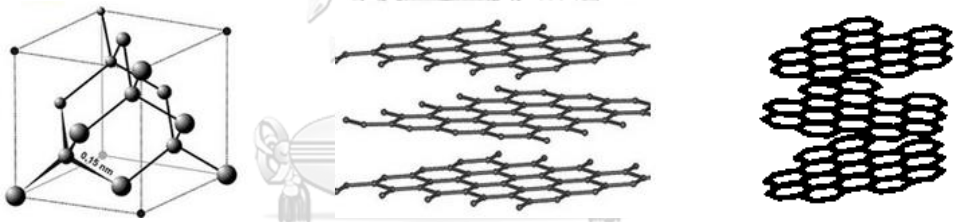

Diamond Graphite Carbon Black

Non-parallel layer planes

Figure 2.6: CB "quasi-graphitic" microstructure compared to the two regular crystalline forms of carbon (diamond and graphite) [37].

2.5.2 Fundamental Properties of Conductive Carbon Black

Particle Size: Electron microscopy shoes CB to be composed of clusters of spherical primary particles, called aggregate or primary aggregates (see Figure 2.7).

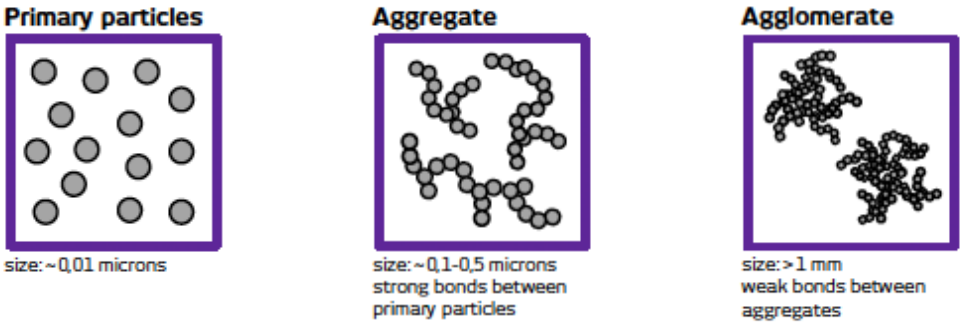

Figure 2.7: CB primary particles fuse together in the reactor and form aggregates and agglomerates [37].

All methods for structure valuation are indirect and essentially consist of measuring the absorbed amount of a suitable chemical, for instance dibutylphthalate DBP. Consequences are expressed in mL or cm^3 (of DBP) absorbed per 100 g of filler. Structure or the DBP adsorbed is function of the aggregates void volumes and defines the degree to which the CB particles have fused together to form aggregates: a low structure CB (low DBP) is made of few primary particles compactly fused together while a high structure CB (high DBP) is made of many primary particles with considerable branching and chaining (see Figure 2.8).

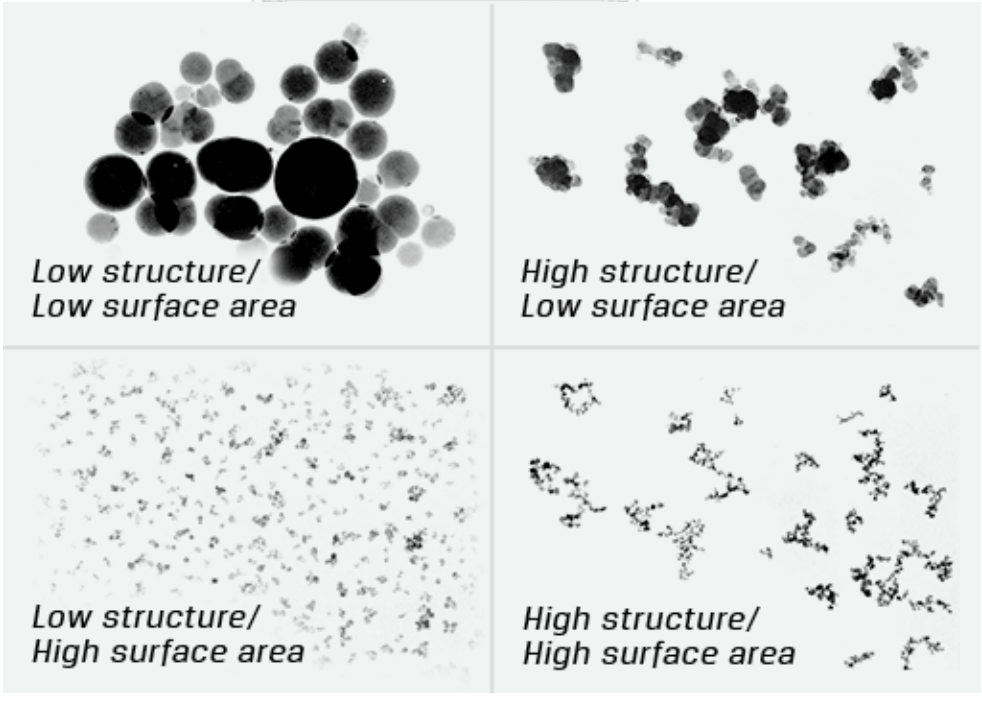

Figure 2.8: Visualization of CB particle size/surface area and structure [37].

The specific surface area is evaluated either through iodine I_2 adsorption (result in m^2/g of I_2 per g of CB), or through nitrogen N_2 adsorption result in m^2/g of CB. Small particles will discuss a high surface area per unit weight so the high surface area is the critical characteristics of CBs that inform electrical conductivity at lower contents in polymer composites.

According to the CB aggregate structure, CBs are categorized into a high structure and a low structure [13]. High structure CB is characterized by additional branching and chaining per primary aggregate compared to the low structure CB. The main disadvantage of the low structure CB-filled polymer composites is the high concentration of CB (~15-20 wt%) required to attain the percolation threshold. Such high filler loading affects the composite mechanical properties, process ability and increases the price of the final composites. Consequently, reducing CB content in conductive polymer composites is a key research challenge. Recently, one of the most common methods to decrease the percolation threshold and electrical resistivity at a relatively low CB content is to use two-component polymer blends as matrix based on the "double percolation" behavior, i.e. the percolation of electrical conductivity in such an immiscible or partially miscible polymer blend depends on the continuity of CB-rich phase or the interface as well as the percolation of CB in CB-rich phase or at the interface. By the preferential localization of CB particles in a distinct region, such as a phase of a dual continuous phase blend or interface between two phases, the effective CB loading was greatly higher than its nominal value, hence the percolation threshold reduced significantly [39].

2.6 Mechanism of Electrical Conductivity

2.6.1 Conductive Path

In the area of low filler volume fraction, the conductive filler particles of different sizes and shapes are dispersed homogeneously into the insulating matrix.

Consequently, there are no contracts between the adjoining filler particles. As the volume fraction of the filler increases, particles come closer and small agglomerates begin to growth. In certain volume fraction i.e. percolation threshold, conducting particles or small agglomerates touches other agglomerates or particles and forms a conductive network inside the conducting particles as shown in Figure 2.9.

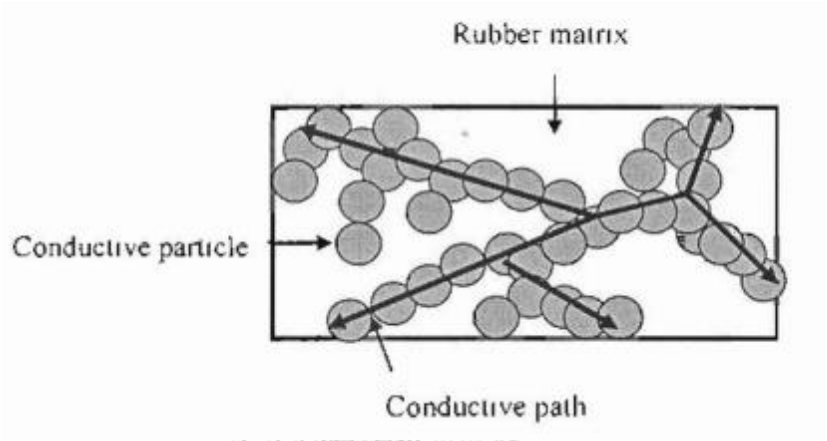

Figure 2.9: Conductive paths in composites without pressure [40].

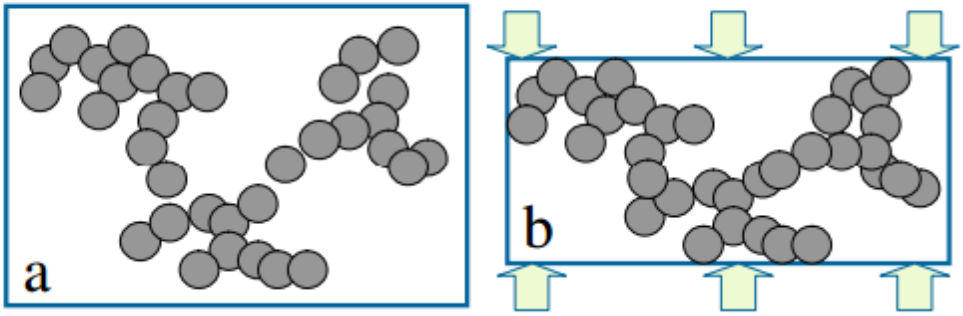

Figure 2.10: Formation of conductive paths in composite by pressing [40].

2.6.2 Effect of Pressure on Resistivity Measurement

The electrical resistance of conductive filler dispersed polymer composite materials depend mostly on applied stress, magnetic field, temperature and humidity. As explained above, at a certain volume fraction of filler, the conductive path is formed in an insulating matrix when the conducting particles come in contact with another

and form one to three dimensional conducting network structure. Nevertheless, when pressure is applies on the composite, the conducting particles originate contact with one another more readily and a conducting path is formed. When the pressure is released, the conducting path is discontinued. The formation of conductive pathways after applying external pressure is shown in Figure 2.10. When the pressure is applied, the conducting path is formed when the volume fraction of filler is less than that of composites without applied pressure i.e. total volume of the matrix declines upon pressure.

2.7 Percolation Theory and Models

Polymers are generally insulating materials. By adding electrically conductive filler, the composites will display electrical conductivity and can be used in a variety of applications. The electrical conductivity of the mixture increases intensely at a critical filler concentration called the percolation threshold. Below this concentration the filler particles are not consistent within the polymer matrix. The composite remains an insulator with no contact between the filler particles. Once the concentration reaches the percolation threshold concentration, the filler particles are able to contact each other, and form a conductive network. Figure 2.11 displays typical electrical conductivity behavior of a polymer filled with conductive filler as a function of filler concentration. It is valuable to note that theoretically expected percolation threshold for a randomly dispersed system is around 15 vol% [41]. Many models and equations have been offered to understand this behavior. Some of these models are reviewed in this section.

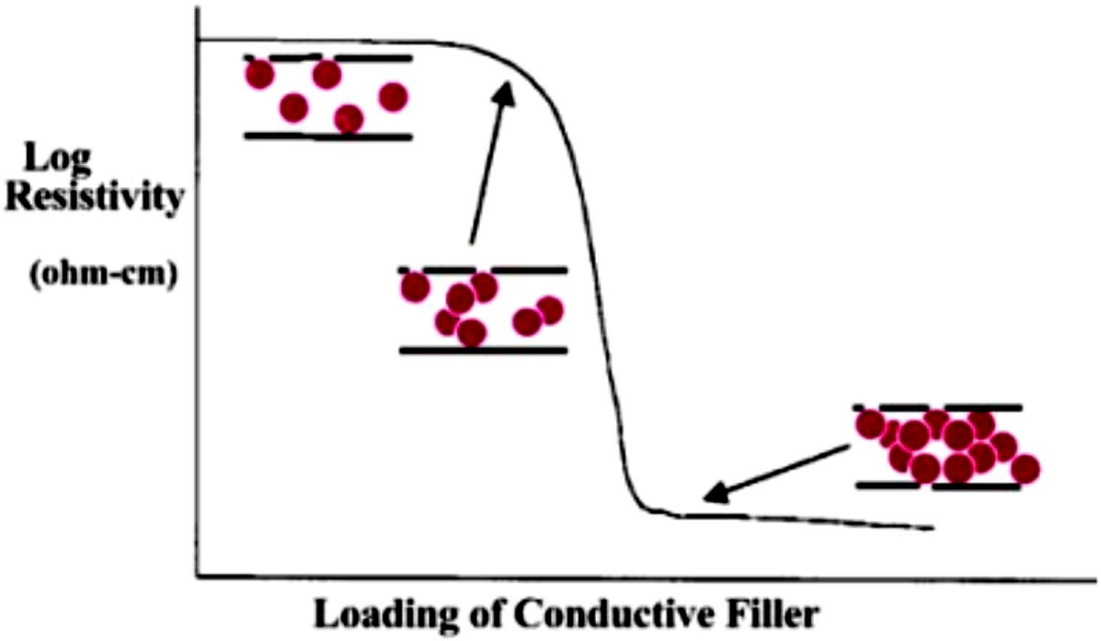

Figure 2.11: Schematic of electrical resistivity as a function of filler loading [42].

Kirkpactrick formalized percolation theory to predict resistivity above the percolation threshold concentration [13, 40]. He showed that electrical resistivity follows the power-law correlation:

$$\rho = \rho_0 (V - V_c)^{-s} \qquad (2.1)$$

where ρ is the composites electrical resistivity (Ω.cm), ρ_0 is the intrinsic resistivity of the filler (Ω.cm), V is the volume fraction of the filler, V_c is the percolation threshold and s is the power-law exponent. The value of s is typically between 1.5 and 3 for three-dimensional percolation.

2.8 Minimization of CB Loading by using Polymer Blend as Matrix

In terms of large-scale practical applications, melt processing, the addition of CB in the single thermoplastic polymeric hosts is interested. However, in most of these

system, V_c remains high because of the high filler content. This system leads to difficulties in processing due to an increase in melt-viscosity of the blends, the high final cost and, poor mechanical properties, such as brittle. It is necessary for the conducting filler content to be as low as possible to achieve good process ability, low cost, and good mechanical properties. The general approach undertaken to reduce to CB content is by the formation of segregated CB structures. Therefore, the dispersion of CB particles in a semi-crystalline polymer, where the CB is localized in the amorphous regions, results in a percolation threshold decrease. Otherwise, binary immiscible or partially miscible blend have been currently received and interest to be utilized in minimizing percolation threshold since heterogeneous morphologies allow the filler preferentially accumulate in certain regions. To attain isotropically conductive materials, multiphase systems, which allow filler to form conductive network within continuous phase are preferred.

The selective location of conducting particles in one of the two phases or at the interface of a co-continuous two-phase polymer blend is a very efficient strategy to decrease the CB percolation threshold [43] (see Figure 2.12, for example). It is worth pointing out that double percolation or percolation-within-percolation is at the original of this location:

- percolation of the polymer phases and thus of their interface and

- percolation of the conductive particles in one phase or at the interface

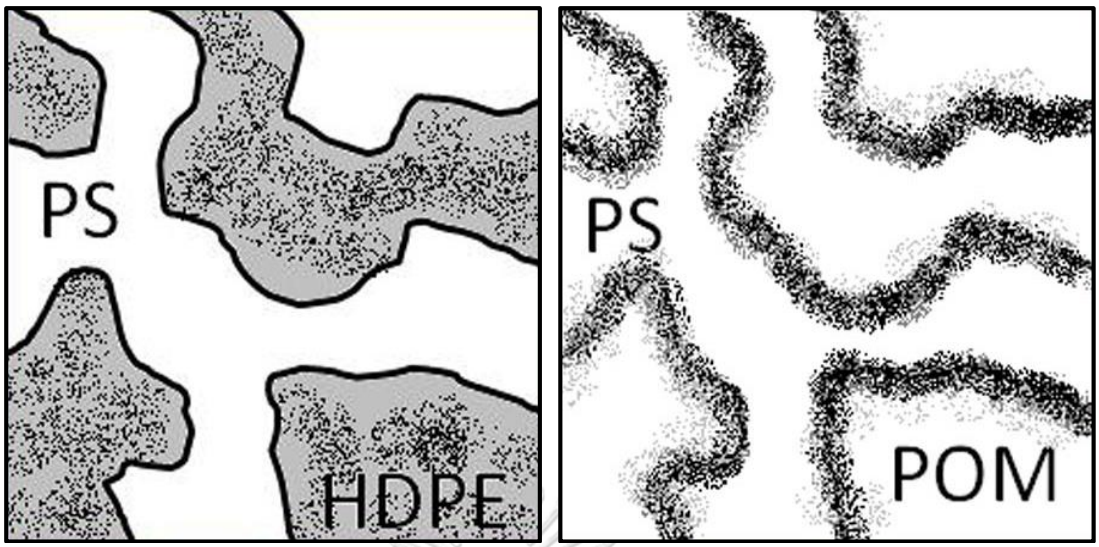

(a) (b)

Figure 2.12: Self-assembly structure model of polymer PS/HDPE blend and PS/POM blend filled with carbon black: (a) CB filled in one phase (HDPE), (b) CB filled in interface [43].

The existence of different CB arranges is given by the following factors [43-45]:

1. Thermodynamic factor: It relates to 'interface tension polymer A-filler, polymer B-filler and polymer. When CB particles blended with the polymer blends consisting of polymers A and B, phase where CB located is predicted by

Young's equation:
$$\omega = \frac{(\gamma_{CB-A} - \gamma_{CB-B})}{\gamma_{A-B}} \quad (2.2)$$

where $\gamma_{CB\text{-}A}$, $\gamma_{CB\text{-}B}$ and $\gamma_{A\text{-}B}$ are, respectively, the interfacial energy between polymer A and CB. between polymer B and CB, and between polymers. ω is catted the wetting coefficient. When

$\omega > 1$	CB particles distribute within the phase
$-1 < \omega < 1$	CB particles distribute at the interface
$\omega < -1$	CB particles distribute within the A phase

In principle the knowledge of the polymer/polymer and of the polymer/filler interfacial tensions should be sufficient to anticipate the morphology. Nevertheless, if experimental data may be found for polymer/polymer interface it is almost difficult to find it for polymer/filler. Generally, they are estimated with the help of theoretical models like the well-known Wu equations [46]:

$$\gamma_{12} = \gamma_1 + \gamma_2 - 2\sqrt{\gamma_1^d \gamma_2^d} - 2\sqrt{\gamma_1^d \gamma_2^d} \qquad (2.3)$$

Only $\boldsymbol{\gamma}_i$ the surface tension of component i need to be known. The exponents d and p stand for respectively the dispersive and the polar contribution to the surface tension.

2. Kinetic factor: It relates to viscosities of the polymer components at the temperature of processing. The CB particles prefer to localize in low viscosity polymer phase.

Mamunya et ai. [43] studied the percolation phenomena in polymers containing dispersed iron. In this research, he explained that the differences are caused by the specific structure of the composite based on the PE/POM blend. Due to the large difference between the polymer melt viscosities of PE and POM (melt flow indexes 1.6 and 10.9 g/10 min, respectively), the filler is located in the POM phase during formation of the filled system from polymer melt in the extruder. So the Fe particles in the PE/POM/Fe composite will be selectively dispersed in the POM phase because of its lower viscosity as shown in Figure 2.13.

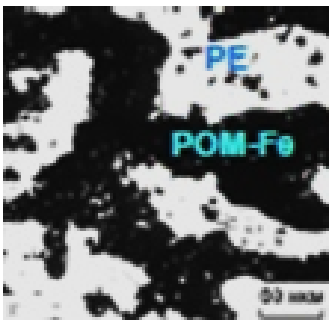

Figure 2.13: Optical microscopy micrographs of the PE/POM-Fe composite [43].

3. Processing factor: It relates to methods of the filler introduction to the complex polymer matrix, which can either enhance or depress influence of thermodynamic and kinetic factors. Generally, filled polymer blends can be prepared by the following five methods [41]:

method A - first the CB is introduced to the polymer 1. then the concentrate of filler in the polymer 1 is diluted by polymer 2;

method B - on the contrary, the concentrate of CB in the polymer 2 is prepared and then is diluted by polymer 1;

method C - all three components are charged to extruder and mixed at the same time;

method D - the filler is mixed with the previously prepared polymer blend;

method E - CB is introduced both in the polymer and polymer 2, which is followed by mixing of the filled polymer components.

Method A-D are two-stages; Method E is one-stage.

It has been reported that the processing sequence is one of the important factors that influence the electrical properties of CB-filled various binary polymer blends [47]. Cui et al. [48] studied the effect of processing sequence on the electrical properties of immiscible PP/Novolac blends filled with CB. The effect of different processing sequence on the electrical properties was investigated in addition to the

simultaneously met moing blends, (Novolac+CB)/PP and (PP+CB)/Novolac blends were prepared by pre-melt mixing CB with Novolac resin (or PP). followed by the addition of PP (or Novolac resin) Table 2.2 displays the volume resistvity of PP/Novolac/CB (70/30/6) blends with different processing sequence. For the PP/Novolac/CB (70/30/6) blends, the volume resistivity of the simultaneously melt blended and the (Novolac+CB)/PP samples is alike. While the volume resistivity of the (PP/CB/Novolac samples are much higher ($2.0x10^{16}$ Ω.crn), it could be conclude that the addition of Novolac into PP/CB increased the volume resistivity. It proposes that the CB particles partially migrate into the Novolac phase, reducing the CB concentration in the continuous PP matrix. It could be a good attraction of Novolac with CB and the strong Novolac/CB interaction that drive CB to interact with the Novolac phase and migrate to another polymer domain.

Table 2.2: Volume resistivity of PP/Novolac/CB (70/30/6) blends with different processing sequences [48].

Sample Composition	Method of Processing	Volume Resistivity (Ω.cm)
PP/Novolac/CB (70/30/6)	Simultaneously melt-blended	7.1×10^{8}
	(Novolac+CB)/PP	4.7×10^{8}
	(PP+CB)/Novolac	2.0×10^{16}

CHAPTER III

LITERATURE REVIEWS

Kapataidakis et al. 1999 [49] studied interrelation between phase state and gas permeation in polysulfone/polyimide blend membranes. We describe the results of the calorimetric studies with respect to the phase state of the blends. Different experiments were done with DSC. In the first experiment, all specimens were heated from ambient temperature to 613 K at a heating rate of 10 K/min. Figure 3.1(a) shows the resulting thermograms. For the homopolymers PSF and PI, two relatively narrow T_g's were obtained, at 461 and 589 K, respectively. For the blends rich in PSF, again a single (albeit broad) T_g was obtained that is higher than that of the pure PSF. For the 50/50 and 20/80 blends, a very broad transition range is observed with some indication of two very broad T_g's, in agreement with the results from rheology. In a second DSC experiment, a second heating run was made (with 10 K/min); the results of the first and second runs are compared in Figure 3.1(b) for the 50/50 blend. Clearly, heating the blend at 613 K results in a complete phase separation into PSF and PI macrophases, as indicated by the two T_g's in the blend being very close to those of the pure components. This was the case with all blends; that is, after heating to 613 K in the second run, two T_g's were evident at identical temperatures to those of the homopolymers. This process was irreversible; that is, at no time was remixing observed. Therefore, during the first heating runs the blends are in a kinetically frozen-in metastable state, which is induced by the solvent. After heating above the T_g, the chains find sufficient mobility and phase separate. This situation for the PSF/PI blend system is very reminiscent of that for the polyethersulfone (PES)/PI blend system studied earlier [46], with one difference. In the PES/PI system, during the first heating a single T_g was observed at all compositions. The two T_g's in our 20/80 PSF/PI blend may originate from the greater dynamic asymmetry (i.e., the greater difference in T_g's) of the homopolymers in the PSF/PI system (ΔT_g's≈140 K) as compared to the PES/PI system (with ΔT_g's≈90 K)

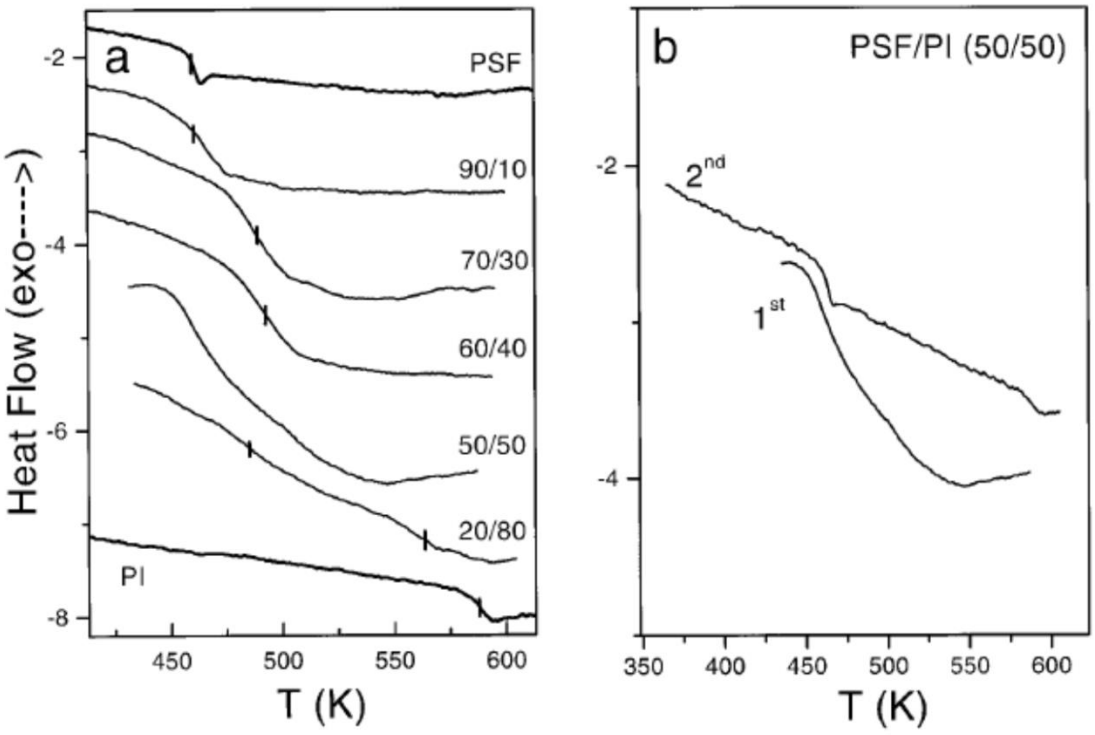

Figure 3.1: (a) DSC thermograms for the homopolymers and their blends taken during the first heating run. (b) Comparison of two thermogramms for the 50/50 PSF/PI blend taken during the first and second heatings [49].

Ammar [50] studied the morphology and mechanical properties of polysulfone/polyimide nanocomposite films. The mechanical properties of PSF/PI blends are presented in Table 3.1. The tensile modulus of specimens with different PSF contents indicated that PSF is also to increase the tensile modulus of PSF/PI. As shown in Table 3.1, when the PSF content increased from 0 to 70 wt%, the tensile modulus of specimens increased from 2436.87 to 3028.59 MPa. The increase of tensile modulus with the addition of PSF was due to the rigidity ability of PSF. Furthermore, the tensile strength of PSF/PI blends formed synergy between strength of PSF and PI, for the tensile strength 30PSF/70PI is the maximum tensile strength in all specimens. However, the elongation at break of PSF/PI blends formed antagonism between elongation at break of PSF and PI.

Table 3.1: The mechanical properties polysulfone/polyimide blend films [50].

Polymer	Modulus (MPa)	Tensile strength (MPa)	Elongation at break (%)
PI	2436.87	49.63	26.70
30PSF/70PI	2847.25	62.37	23.91
50PSF/50PI	2440.39	36.13	20.87
70PSF/30PI	3028.59	55.94	22.69
PSF	3053.90	28.42	26.8

Linares and Benavente [51] studied the effect of sulfonation on thermal, mechanical, and electrical properties of blends based on polysulfones. All specimens, including the ternary blend, display a single T_g, which varies as a function of blend composition. In the case of DMA measurements, the glass transition temperature was obtained from *E"*-maximum (Figure 3.2) because it provides similar information than tan δ, but the different relaxation processes are more evident, and it relates much better to the value obtained by DSC [52]. Both techniques give analogous results indicating that, a priori, we are dealing with blends, which, at least from a macroscopic point of view, behave like totally miscible.

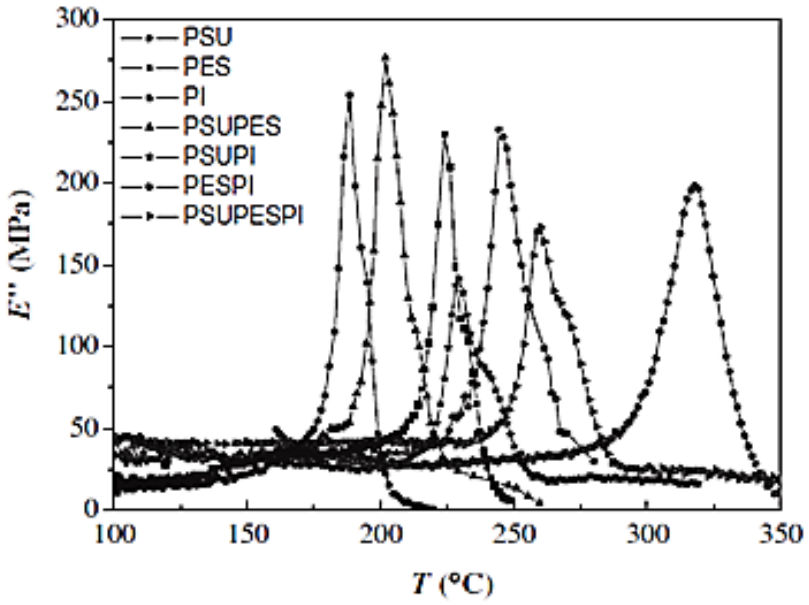

Figure 3.2: Loss modulus of PSU (●), PES (■), PI (◑), PSUPES (▲), PSUPI (★), PESPI (◓), and PSUPESPI (▶) [51].

Gao et al. [53] studied the high-performance conductive baterials based on the selective location of carbon black in poly(ether ether ketone)/polyimide matrix. The effect of CB content on the conductivity of the TPI/CB, PEEK/CB and PEEK/PI/CB is shown in Figure 3.3. The TPI/CB composites exhibit in the same manner as the PEEK/CB composites, the increase in conductivity at a well-defined threshold of incorporated CB to 10 wt% of combined CB. At CB contents greater than 10 wt%, the rate in increase of conductivity with increasing CB content is reduced. Furthermore, the TPI/CB composites have a significantly lower conductivity, relative to the PEEK/CB system, at CB concentration levels past the PEEK/CB percolation threshold. A contributing factor to the large disparity in the conductivity characteristics of these systems is the relative difference in the surface tension and polarity of the polymers. TPI is characterized by a higher surface tension and polarity compared to that of PEEK, both of which have been shown to promote higher CB percolation thresholds. The percolation threshold of PEEK/CB was observed at 5-8 wt% CB. The percolation threshold of the PEEK/TPI/CB

composites is between 2.5 and 4.0 wt% CB where the conductivity changes by 3 orders of magnitude. This threshold is at a significantly lower CB content than the individually filled PEEK or TPI. From the results, it could be concluded that the usage of polymer blend can be reduced CB in composites.

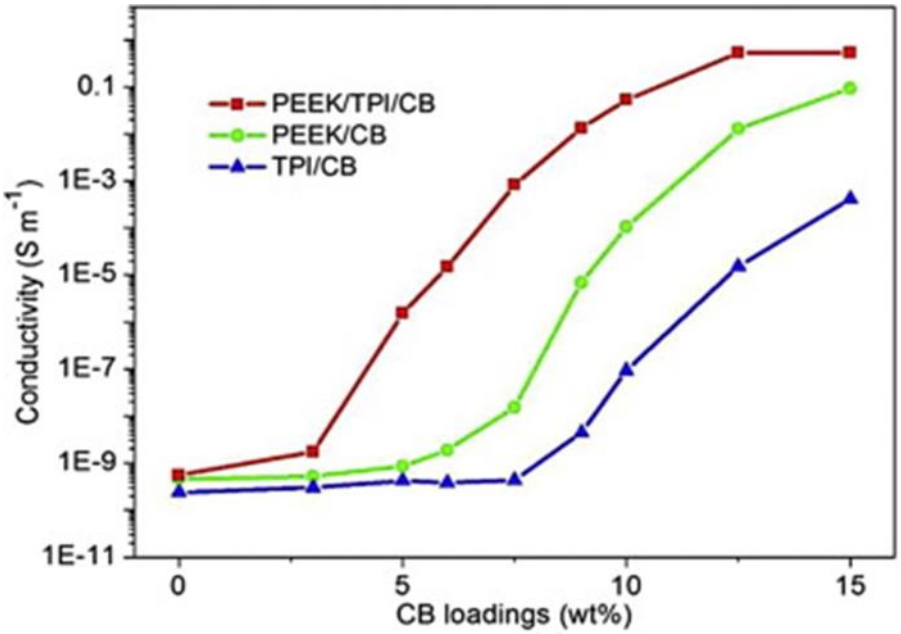

Figure 3.3: Conductivity of PEEK/TPI/CB composites (■), PEEK/CB composites (●), and TPI/CB composites (▲) [53].

The thermo-degradation curves of PEEK/TPI blend and PEEK/TPI composites with different contents of CB are shown in Figure 3.4. It can be seen that the thermal stability of PEEK/TPI/CB composites were much superior compared with that of PEEK/TPI blend. The 5% and 10% weight loss temperature ($T_d^{5\%}$ and $T_d^{10\%}$) of PEEK/TPI blend were 557°C and 583°C, whereas the $T_d^{5\%}$ and $T_d^{10\%}$ of PEEK/TPI composite with 5 wt% CB reached 571°C and 589°C, respectively. This may attributed to CB restricting of thermal mobility of polymer chains, thereby making the composites more thermally stable [54]. Simultaneously, the selective location of CB and the formation of the co-continuous structure might also benefit the thermal stability of the PEEK/TPI/CB

composites. Moreover, the PEEK/TPI composite with 10 wt% CB presented excellent thermal stability, the $T_d^{5\%}$ and $T_d^{10\%}$ were 583°C and 597°C respectively, which was 26°C and 14°C higher than that of PEEK/TPI blend without CB. These results indicate that the incorporation of CB could improve the thermal stability of PEEK/TPI blend effectively, the $T_d^{5\%}$ under air atmosphere of PEEK/TPI/CB composites was all above 571°C, which indicated the outstanding thermal stability of this material.

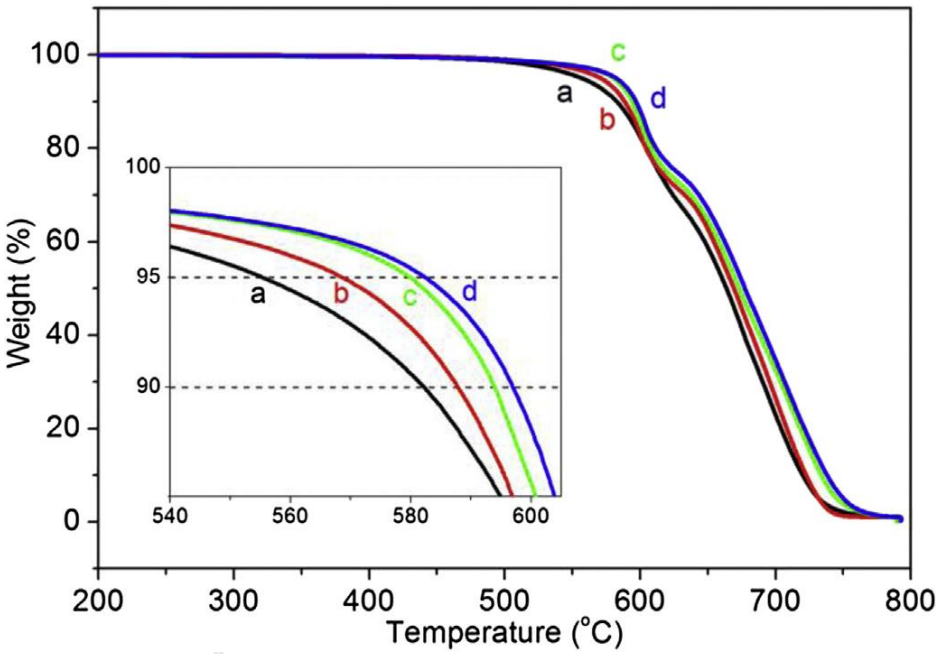

Figure 3.4: TGA curves of (a) P/T, (b) P/T/5%-CB, (c) P/T/7.5%-CB and (d) P/T/10%-CB [55].

Table 3.2: DMA curves of (a) P/T, (b) P/T/5%-CB, (c) P/T/7.5%-CB and (d) P/T/10%-CB [55].

Specimen names	Tensile strength (MPa)	Elongation at break (%)
P/T	102	8.6
P/T/5%-CB	90	7.9
P/T/7.5%-CB	92	7.2
P/T/10%-CB	75	5.0

Apart from the satisfying thermal enhancement, the mechanical properties of the PEEK/TPI/CB composites were investigated by typical tensile test, as shown in Table 3.2. In general, any heterogeneity or aggregation of CB could result in structural defects with detrimental effects on the mechanical properties [56, 57]. Therefore, the tensile strength and elongation at break of the composites both decreased with increasing contents of CB. On the other hand, the changes of the tensile modulus with temperature can be investigated by dynamic mechanical analysis (DMA). Storage modulus measured by DMA is regarded as the maximum energy stored in the material during one cycle of oscillation, and represents the stiffness and elastic nature of the material. The variation of the storage modulus curves as a function of the temperature for PEEK/TPI blend and its CB composites are presented in Figure 3.5. The storage modulus values of the PEEK/TPI/CB composites were obviously higher than that of neat PEEK/TPI blend in the temperature range of 50-240°C. With increasing the CB loadings, the storage modulus of the PEEK/TPI/CB composites increased gradually. Take the temperature range of 50-150°C for example, the storage modulus of PEEK/TPI blend was about 1830 MPa, while the storage modulus of PEEK/TPI/CB with 5 wt% of CB reached around 2264 MPa, and it continued to increase to 2456 MPa and 2660 MPa with 7.5 wt% and 10 wt% CB, respectively. The reinforcement in storage modulus of PEEK/TPI/MWCNTs should ascribed to the formation of continuous TPI networks and the selective location of CB particles in TPI phase [24].

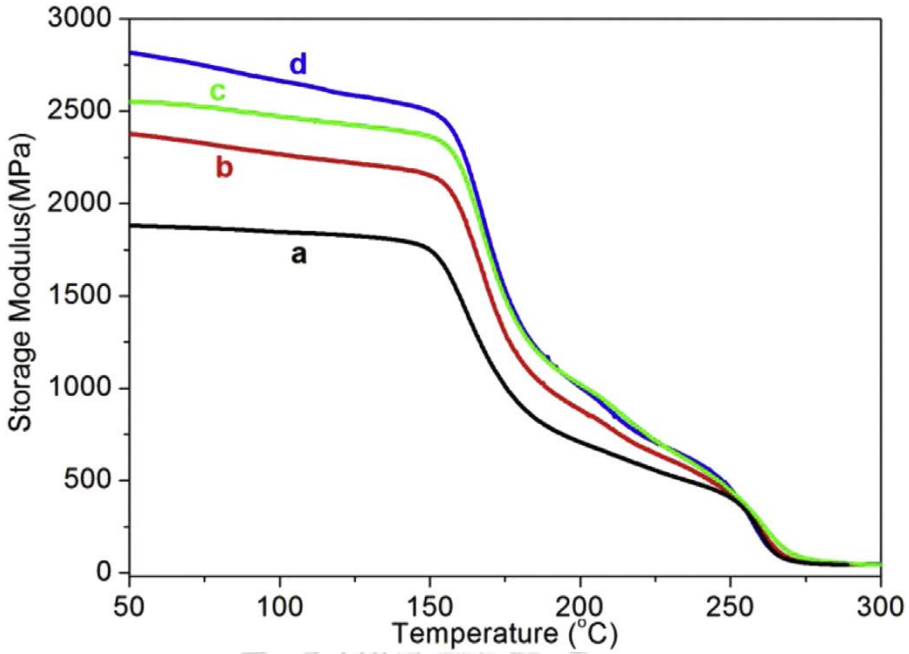

Figure 3.5: DMA curves of (a) P/T, (b) P/T/5%-CB, (c) P/T/7.5%-CB and (d) P/T/10%-CB [53].

Zhang et al. [58] studied two-step positive temperature coefficient effect with favorable reproducibility achieved by specific “island-bridge” electrical conductive networks in HDPE/PVDF/CNF composite. The conductive mechanism of HDPE/PVDF/CNF composites with various electrical conductive networks induced by different component ratios of binary-polymer, SEM micrographs of HDPE/PVDF/CNF (f_{CNF} = 3 vol.%) were observed and the results are shown as Figure 3.6. From the SEM micrographs shown in Figure 3.6a–c., two distinct regions are observed, one is the HDPE containing CNF sand the other is PVDF free of CNFs. When the volume ratio of HDPE and PVDF is 1:4, obvious “sea-island” structure, namely HDPE phase containing CNFs as the dispersed phase while PVDF phase forming the continuous sheath structure, is formed in the composites (Figure 3.6a). It should be noticed that although most of the CNFs are localized in HDPE phase, a considerable amount of them can be observed in PVDF phase shown as the red circle marked area in Figure 3.6d. Meanwhile, some CNFs localized in HDPE phase can be found stretched out partly from the island. Based on the SEM micrographs, we can describe the electrical conductive network as shown in

Figure 3.6g. Most of the CNFs are distributed in HDPE phase and form very dense electrical conductive island. These CNFs then act as bridges and link the adjacent conductive islands, forming the three-dimensional electrical conductive network penetrated throughout the whole composites. We name this distinct electrical conductive network structure as “island-bridge” structure, networks there. As a result, the islands separated by the continuous PVDF phase are highly conductive (Fig. S1a). While, not all the CNFs can be contained by HDPE phase because the ratio of HDPE is relatively low and there will be a considerable number of CNFs are left in PVDF phase and some CNFs can stretch partly from the HDPE.

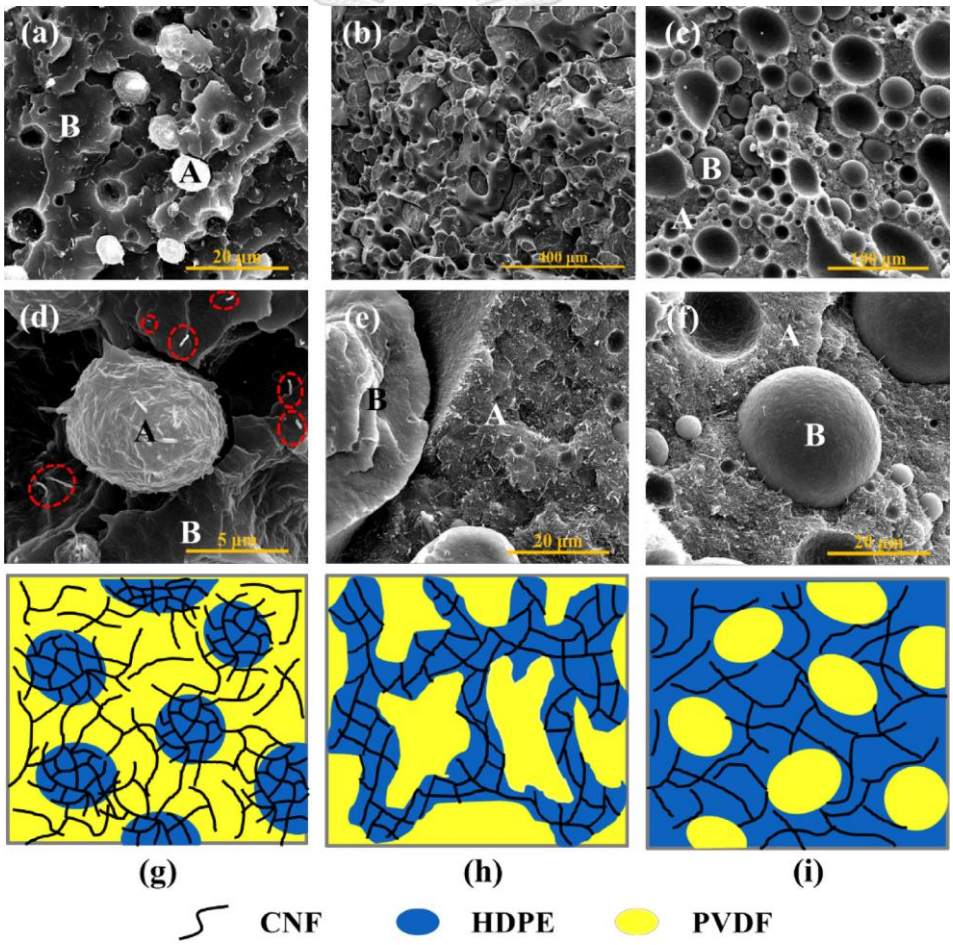

Figure 3.6: SEM micrographs and schematic images of conductive mechanism for 3 vol.% CNF filled HDPE/PVDF/CNF composites with different volume ratios of binary-polymer. (a, d, g) 1:4, (b, e, h) 1:1, (c, f, i) 4:1, region A is CNF filled HDPE phase and region B is PVDF phase. [58].

As shown in Figure 3.6b and e, the conductive CNFs are preferentially localized in HDPE phase and form a continuous network structure, and the HDPE phase is also continuous in three-dimensional space. In other words, a double-percolated structure is formed in the composites when the volume ratio of HDPE and PVDF is 1:1. In this situation, the content of HDPE is high enough to contain all the CNFs so that there are hardly any CNFs could be observed in PVDF phase in Fig. 4b and e. The existence of PVDF helps to increase the concentration of CNFs in HDPE phase. The electrical conductive network of CNFs is only existed in HDPE phase and the conductive phase penetrates the entire composites, which can be named as a trinary-continuous structure in three-dimensional space (see Figure 3.6h). With the further increase of HDPE, PVDF phase acts as nonconductive islands for absence of CNFs there and CNFs filled HDPE phase is the continuous phase. The content of HDPE is rather large in this situation resulting in the dilution of CNFs localized there. Therefore, the electrical conductive network in the composites (see Figure 3.6i) is not as dense as that of the composites with ternary-continuous structure.

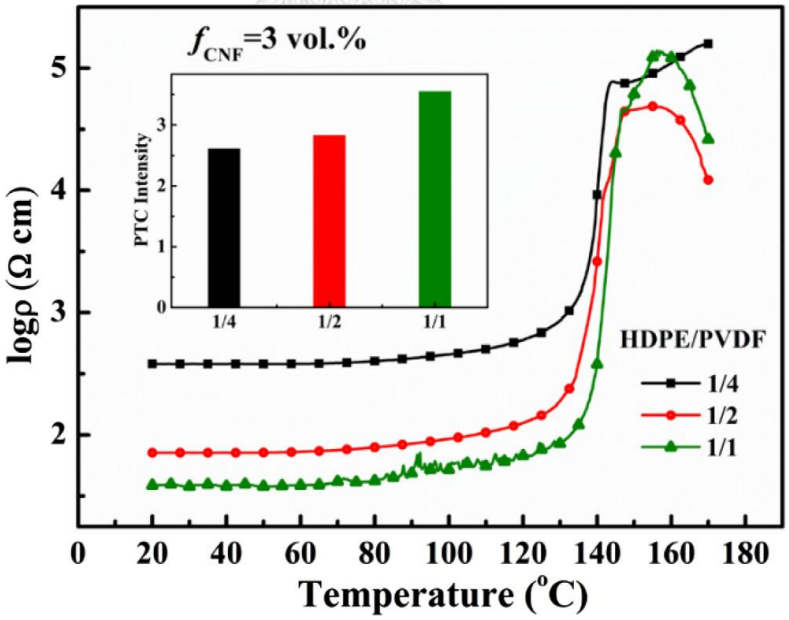

Figure 3.7: Temperature dependence of resistivity for 3 vol.% CNF filled HDPE/PVDF/ CNF composite with different volume ratios of HDPE and PVDF(1:4, 1:2, 1:1). Inset: PTC intensity of the composites correspondingly.

The temperature dependence of resistivity of HDPE/PVDF/CNF composites with various morphologies during heating process shown in Figure 3.7. The change of resistivity at relatively low temperature is not obvious, while the increase of resistivity is very sharp when the temperature is close to the HDPE melting point which is consistent with our viewpoint above concerning the preferential location of the conductive fillers in the HDPE phase.

Also, there are many differences in the PTC behavior for the composites with different morphologies, indicating that the PTC effect is dependent on the constituents of the matrix. First, the initial resistivity is significantly different for the three kinds of composites and the highest one is found in the composite with PVDF phase as the main part. When the HDPE phase filled with CNFs becomes continuous from dispersed phase, the resistivity decreases a lot. When the double-percolated structure is formed (the volume ratio of HDPE and PVDF is 1:1), the initial conductivity is the highest among all the composites. This phenomenon is caused by different electrical conductive networks.

CHAPTER IV
EXPERIMENTAL

4.1 Materials

3,3′,4,4′-biphenyltetracarboxylic dianhydride (*s*-BPDA), 4,4′-diaminodiphenyl ether (ODA), and polysulfone resin (PSF) were purchased from Sigma-Aldrich. 1-Methyl-2-pyrrolidone (NMP) and 1,3-Dimethyl-2-immidazolidinone (DMI), the solvents for poly (amic acid) synthesis, were purchased from Fluka and TCI, respectively.

4.2 Sample Preparation

4.2.1 *s*-BPDA/ODA Poly(amic acid) Preparation

s-BPDA/ODA polyimide was synthesized by the condensation polymerization via a conventional two-step method, consisting of polymerization of a soluble poly(amic acid) (PAA) intermediate. This synthesis is based on the reaction of ODA with *s*-BPDA in a polar aprotic solvent, i.e. NMP or DMI, at room temperature. The resulting poly(amic acid) was then cyclized by thermal imidization in a subsequent heat treatment to produce the desired polyimide films.

4.2.2 Polyimide Blend Preparation and Imidization Condition

PAA solution based on *s*-BPDA and ODA was prepared in NMP, whereas PSF solution was made by dissolving of PSF resin in NMP. Solution mixture of the polymer blends and CB-filled PI/PSF blends were prepared by measuring calculated mass of PAA solution, PSF solution, and CB followed by a thorough mixing at room temperature to obtain a clear and homogeneous solution mixture. The measured amount of the resulting clear solution mixture was then casted on to a glass substrate. The mixture was dried in an air-circulated chamber at room temperature for 1 hour and at 60°C for

8 hours. The imidization was performed stepwise in vacuum oven using the heating program at 150°C for 1 hour, 200°C for 1 hour, and 300°C for 1 hour. Then the films with the thickness of 100 μm were cooled to room temperature and removed from the glass substrate.

4.3 Characterization of Blend Films

4.3.1 Fourier Transform Infrared Spectroscopy (FTIR)

Fourier transform infrared spectroscopy (FTIR) spectra of polyimide blend films were recorded using a Perkin Elmer Spectrum GX FTIR spectrophotometer. The scan number and the spectral resolution were 64 and 8 cm^{-1}, respectively. Absorbance spectra were then obtained

4.3.2 Rheological Property Measurement

Rheological properties of neat PI and PSF were examined by using Rheometer (ARES G2, TA Instrument) equipped with 25 mm parallel plate geometry. The measuring gap was set at 1 mm and the experiment was performed under a dynamic frequency sweep mode using frequencies ranging from 0.1 to 100 Hz at constant temperature 30°C. All samples are preheat for 5 minutes before testing.

4.3.3 Dynamic Mechanical Analysis (DMA)

Dynamic mechanical analyzer (DMA) model DMA 224 from NETZSCH Instrument was used to investigate dynamic mechanical properties. The dimension of specimen was 5 mm × 23.7 mm × 0.05 mm (W×L×T). The test was performed under the tensile mode. The applied strain amplitude was 0.3% at the deformation frequency of 1 Hz. The specimen was heated using a temperature ramp rate of 3°C/min under nitrogen atmosphere from room temperature to 350°C. The glass transition temperature was

taken as the maximum point on the loss modulus curve in the temperature sweep tests. The storage modulus (E'), loss modulus (E''), and loss tangent (tanδ) were then attained. The glass transition temperature (T_g) was taken as the maximum point on the loss modulus curve in the DMA thermograms.

4.3.4 Density Measurment

The density of each specimen was determined by water displacement method according to ASTM D 792 (Method A). All specimens were prepared in a rectangular shape (50 mm × 25 mm × 2mm). All specimen was weighed in air and in water at 23±2°C. The density was calculated using Equation (4.1). An average value from at least five specimens was calculated.

$$\rho = \left[\frac{A}{A-B}\right] \times \rho_0 \qquad (4.1)$$

where ρ = density of the specimen (g/cm^3)

A = weight of the specimen in air (g)

B = weight of the specimen in liquid (water) at 23±2°C (g)

ρ_0 = density of the liquid (water) at the given temperature (g/cm^3)

The measurement was carried out using five specimens per formulation and the average value of the sample was obtained.

4.3.5 Electrical Property Measurement

Electrical resistivity measurements were conducted using two different instruments. At least three samples were tested for each formulation. An Electrometer (4284A, HP) was used to perform room temperature resistivity measurements on specimens with resistivity lower than 10^6 Ω.cm, while a high resistance meter (6517A,

Keithley) was used for specimens with higher resistivity. An average electrical value from of about 3 readings was reported. All specimens are tested under a voltage of 2 V.

4.3.6 Tensile Property Measurement

Tensile modulus and tensile strength of polyimide blend films were determined using a universal testing machine (model 5567) from Instron Instrument. The test method used was a tension mode with a specimen dimension of 8.0 cm × 0.50 cm × 0.025 mm and the specimen gauge length of 4.0 cm. The testing crosshead speed was 0.50 cm/min. The tensile properties were obtained following the general procedure in ASTM D882 using five specimens per test condition.

4.3.7 Thermogravimetric Analysis (TGA)

Thermogravimetric analyzer model TGA1 from Mettler Toledo (Germany) was used to investigate degradation temperature (T_d) and char yield of PI/PSF/CB. The specimen mass used was about 15 mg. The heating rate was 10°C/min from room temperature to 900°C with nitrogen purging flow rate of 100 mL/min. Weight loss of a specimen was measured as a function of temperature. The degradation temperature at 5% weight loss and solid residue of each specimen determined at 900°C were recorded for each formulation.

4.3.8 Optical Microscope (OM)

Optical microscope (OM) model AXIO Scope.A1 from ZEISS was used to investigate phase morphology of PI/PSF blends and PI/PSF/CB composites with objective lens of 10 and 20 magnifications. The obtained micrographs were used to evaluate the selective distribution of CB in PI/PSF blends.

CHAPTER V
RESULTS AND DISCUSSION

5.1 Fourier Transform Infrared Spectroscopy (FTIR) of PAA, PI, PSF, and PI/PSF Blends

Figure 5.1 shows the IR spectra for monitoring the advancement of the poly(amic acid) imidization reaction. From the figure, the characteristic peaks of the poly(amic acid) at 1720 cm^{-1} for carboxylic acid group (COOH), at 1660 cm^{-1} for carbonyl group (C=O) in CONH, and at 1540 cm^{-1} for C-NH stretching band were clearly presented upon 60°C treatment. By increasing the treatment temperature above 150°C, the *s*-BPDA/ODA ring-closing reaction led to the formation of the polyimide as indicated by the substantial decrease of the above characteristic poly(amic acid) bands. The polyimide formation was also identified by observing at 1775 cm^{-1} (the imide bands) for symmetrical carbonyl stretching vibrations, at 1720 cm^{-1} for asymmetrical carbonyl stretching vibration, at 1380 cm^{-1} for stretching vibrations of C-N, and at 740 cm^{-1} for cyclic carbonyl bending vibrations. These absorption bands were clearly observed above 150°C; this could imply that the imidization proceeded to occur mostly at approximately 150°C. Nearly complete imidization was observed after the treatment step leading to the formation of a carbonyl group as identified by the appearance of its absorbance band at 1720 cm^{-1}, which is also overlapped with that of the carboxylic acid of poly(amic acid). Further heat treatment at 300°C for 1 hour revealed no significant changes in the IR spectra. This result is also consistent with those reported by Gardner, Nah et al., and Yang [59-61]. Figure 5.2 shows that C-NH stretching band of the blends were decreased with the increase of PSF leading to the change of ordering and charge transfer having the effect on the PI packing pattern i.e. greater amount of mixed layer packing than preferred layer packing [62].

5.2 Rheological Properties of Neat PI and PSF

According to Paul and Barlow relation [36], Equation 5.1, the ratio of viscosity of polymer 1 and polymer 2 to generate co-continuity phase is shown as follows:

$$\frac{\phi_1}{\phi_2} = \frac{\eta_1}{\eta_2} \quad (5.1)$$

where η_i and ϕ_i are the viscosity and volume fraction of polymers, respectively.

In general, the viscosity ratios or the blending ratios of two polymers depend on the shear rate during operation. Different processing methods (ie. stirring, compression, extrusion and injection) could lead to different shear rates. Therefore, the volume ratios of blending between two polymers to form co-continuous phase are different. For the stirring methods, the shear rates of processing are in the range of 1-10 s^{-1} while those of extrusion methods are in the range of 10-100 s^{-1} [63].

Complex viscosities of PI and PSF as a function of shear rate measured at 30°C were shown in Figure 5.3. From this figure, it was observed that viscosities of PI and PSF decreased with increasing shear rate, suggesting non-Newtonian behavior of a shear thinning type of these polymers. As can be seen, the viscosity of PSF is higher than that of PI over all frequency ranges. Our rheological results revealed that the viscosity values of PI and PSF at low shear rate (1 s^{-1}) were 26.7 and 47.8 Pa.s, respectively; the viscosity values at high shear rate (100 s^{-1}) were 25.0 Pa.s and 32.5 Pa.s, respectively. Therefore, the ratios of the PI/PSF viscosity at low shear rate and high shear rate were 0.56 and 0.77, respectively. According to Paul and Barlow's equation, the calculated volume ratios of PI/PSF at low shear rate and high shear rate were 36/64 and 44/56, respectively.

5.3 Dynamic Mechanical Analysis (DMA) of PI/PSF Blends

Storage modulus (E′), loss modulus (E″) and loss tangent (tan δ) obtained from DMA tests were utilized to characterize PI, PSF and PI/PSF blend at a weight ratio of 40/60 as shown in Figure 5.4-5.6. The storage moduli of PI, PSF and PI/PSF blend at a mass ratio of 40/60 wt% are shown in Figure 5.4. According to the thermograms, storage modulus at room temperature of PI was determined to be 1.80 GPa while that of PSF and PI/PSF blend ratio of 40/60 were about 3.70 GPa and 2.60 GPa, respectively. The storage modulus at room temperature of the PI/PSF blend was observed to increase with the presence of PSF in the blend due to the fact that PSF is more rigid than PI. Furthermore, they exhibited two-step changes corresponding to the positions of glass transition temperature (T_gs) of the PI and PSF phases. From the figure, the positions of T_gs of both PI and PSF phases in the blend were also found to slightly shift towards each other. The above characteristics suggest partially miscible nature of this PI/PSF blend. Furthermore, the greater change in slope of the storage modulus curve vs. temperature of PSF compared to that of PI is one parameter indicating better thermal stability of the PI compared to the PSF and their blend.

Glass transition temperatures of PI, PSF and PI/PSF blend at a weight ratio of 40/60 were determined from the DMA thermograms based on the peaks of loss modulus. In principle, a miscible polymer blend usually exhibits single glass transition temperature (T_g). Whereas in a partially miscible blend, two T_gs of each starting polymer component will be observed and the T_g of each component usually shifts towards each other as a function of blend composition. In the case of immiscible blend, two T_g values can be detected which are the T_g values of the two starting polymers [49, 54]. Figure 5.5 illustrates the loss modulus curves of PI. PSF and PI/PSF blend. From the peak position in each curve, the thermograms of the neat PI clearly revealed a single T_g at 212°C, while that of PSF showed a single T_g at 172°C. Additionally, from this figure, the PI and PSF mixture clearly gave two T_gs which shifts towards each other since the two materials are partially immiscible in nature as

mentioned earlier. In addition, Figure 5.6 exhibits a-relaxation peaks of the loss tangent (tan δ) of the PI, PSF and their blend. From this figure, it was found that the peak maxima of the loss tangent showed the same characteristics as observed in the loss modulus peaks for PI. PSF and the partially miscible PI/PSF blend though at relatively higher values of the corresponding peak positions.

5.4 Morphology of PI/PSF Blends

To investigate the phase morphology of the PI/PSF blends by optical microscope (OM). Figures 5.7a-5.7d show CB-filled PI/PSF blends at the weight ratios 100/0, 50/50, 40/60 and 30/70. The discontinuous PSF domains in PI matrix were observed in the PI/PSF blends with PSF of less than 40% by weight. The PSF domain shape had been changed from small oval shape to more elongated shape with increasing fraction of PSF as shown in Figure 5.7a-5.7b. Moreover, For the PSF filled PI blends of greater than 50% by weight (Figure 5.7c-5.7d); the increase of PSF resulted in the formation of PSF continuous structure as seen in the figure. In this PSF contents of 40% by weight, both PI domains and PSF domains tended to form continuous structure in the continuous PI matrix, which is known as co-continuous phase structure. Consequently, the co-continuous phase can be obtained and can be used as a platform to produce a "double percolation" morphology when CB is added. This double percolation structure is one of the most promising methods to reduce the percolation threshold and to enhance the composite conductivity at lower loading of conductive filler [12, 21-27, 53].

5.5 Density Measurement of CB-Filled PI/PSF Blends

Density measurement of CB-filled PI/PSF blends was performed to examine the presence of void in the specimens. The densities of PI/PSF blends at the weight ratios ranging from 100/0 to 10/90 with CB as conductive filler ranging from 0 to 20 wt%

comparing with their theoretical densities are shown in Table 5.2. The densities of PI/PSF/CB composites are determined experimentally by water displacement method (ASTM D792) and Equation (5.2) by averaging the value from seven specimens whereas the theoretical densities of the PI/PSF/CB composites were calculated from Equation (5.1)

$$\rho = \left[\frac{A}{A-B}\right] \times \rho_0 \qquad (5.2)$$

where ρ = density of the specimen (g/cm^3)

A = weight of the specimen in air (g)

B = weight of the specimen in liquid (water) at 23±2°C (g)

ρ_0 = density of the liquid (water) at the given temperature (g/cm^3)

The theoretical density of PI/PSF/CB composites can be calculated as follow

$$\text{Theoretical density} = (\rho_{PI}V_{PI}) + (\rho_{PSF}V_{PSF}) + (\rho_{CB}V_{CB}) \qquad (5.3)$$

where ρ_{PI} = density of polyimide (g/cm^3)

ρ_{PSF} = density of polysulfone (g/cm^3)

ρ_{CB} = density of carbon black (g/cm^3)

V_{PI} = polyimide volume fraction

V_{PSF} = polysulfone volume fraction

V_{CB} = carbon black volume fraction

The densities of all PI/PSF/CB composites were observed to increase systematically with increasing CB contents following a rule of mixture and the values are compared in Table 5.2. From the table, the measured densities are in good agreement with the theoretical values in all PI/PSF/CB composites with an error of less than 1% (i.e. the densities of PI/CB composites at CB content ranging from 0 to 20 wt% comparing with their theoretical densities are shown in Figure 5.8). From the result, it can concluded that these polymer blends contained negligible void in the obtained specimens.

5.6 Effects of Blend Ratios on Electrical Properties of CB-Filled PI/PSF Blends

Figure 5.9 depicts a relationship between volume resistivity and PSF content of CB-filled PI/PSF blends at a fixed CB content of 1 wt%. The corresponding numerical results in each single polymer PI (i.e. 100%PI or 100%PSF) are summarized in Table 5.3. Although both polymers contained 1 wt% CB, the materials are clearly insulators with the volume resistivity higher than 10^{11} Ω.cm [25]. For the PI/PSF blends at weight ratios ranging from 50/50 to 30/70, the CB-filled PI/PSF blends were found to be evidently more conductive and their volume resistivity values exhibited a minimum value of 5.0×10^{4} Ω.cm at the PI/PSF blend ratio of 40/60 indicating the highest conductivity as seen in Figure 5.9. When increasing the PSF fraction greater than 60 wt%, the volume resistivity tended to increase due to the dilution of the constant amount of CB localized in the PI phase. It is likely that a double percolation effect could take place in the blends containing PSF of about 60 wt% or in this vicinity when the total CB content was 1 wt% in the PI/PSF blends. This result is in good agreement with the work reported by Kwon and coworkers in the PI blends filled with CB [64] and Gao and coworkers in the PEEK/PI blends filled with CB [55]. They reported the increasing amount of the minor phase polymer of partially miscible or immiscible blends, which contains conductive filler lead to double percolative behavior. The volume resistivity of the blends could exhibit a minimum value at the point around

the co-continuous phase morphology when the amount of the conductive filler was constant.

5.7 Electrical Properties of PI/PSF/CB Composites

Figure 5.10 shows the volume resistivity of CB filled PI and PI/PSF blends. All the composites exhibited typical characteristics of percolation phenomenon. The corresponding numerical results were summarized in Table 5.4. At low CB loadings, a little change in volume resistivity could be observed because the distances between CB particles were large enough. The increase of CB content made particles more crowded, leading to the slow decrease of volume resistivity. The volume resistivity decreased dramatically, in the vicinity of the percolation threshold, where the transition from insulating to conductive materials occurred. This indicates CB particles came into contact with each other or closed up enough to allow the electron hopped by tunneling, thus forming continuous conducting paths or network. Once the percolative network was formed, additional CB loading could not significantly reduce the volume resistivity because of the formation of conducting paths [65-67]. The percolation threshold of CB filled polymers, in our case, was determined at the volume fraction of CB that the compounds change from insulative behavior (>10^{11} Ω.cm) to conductive behavior (<10^{4} Ω.cm) [39].

In CB added PI/PSF blend systems, the percolation threshold depend strongly on the phase morphology and the distribution of CB in the polymer blends. Figure 5.10 shows the volume resistivity curves of PI/PSF blends at the weight ratios between 100/0 and 40/60 with CB as conductive filler ranging from 0 to 20 wt%. It was observed that the percolation threshold of CB-filled PI is about 2-8 wt% CB. The percolation regions of the PI/PSF-based composites were lower than those of PI-based composites and they were shifted to the left. For example, PI/PSF For mixtures at 60 wt% PSF with 1 wt% CB provided a volume resistivity of about 10^{3} Ω.cm, which was a much lower than that of the PI/CB systems. The percolation threshold of PI/PSF mixtures at 60 wt%

PSF was observed at about 0.2-2 wt% CB, where the volume resistivity changed by 7.8 orders of magnitude. To achieve the volume resistivity of less than 10 ohm, the CB content in the blend can be reduced at least 25% compared to the composite using neat PI as a matrix.

5.8 PTC Behaviors of PI/PSF/CB Composites

Figure 5.11 shows the positive temperature coefficient behaviors of CB filled PI/PSF blends at 40/60. The composite exhibited typical characteristics of percolation phenomenon. At low temperature (<180°C), a little change in volume resistivity could be observed because this temperature range was lower than the glass transition temperature of composite. The increase of temperature made particles move away from conductive network, leading to gradual increase in volume resistivity. In the vicinity of the glass transition threshold, the volume resistivity increased dramatically. The transition from conductive behavior to insulative behavior occurred in this region. This indicates CB particles moved out to inhibit the electron hop, thus conducting paths or networks were lost. The transition threshold of temperature, in our case, was determined at the temperature that the resistivity changed from 10^4 Ω.cm to 10^6 Ω.cm [58].

The PTC repeatability of CB-filled PI/PSF blend, the curves of PI/PSF/CB composites during heating process depended on the stability in the polymer composite. Figure 5.9 shows the volume resistivity curves of PI/PSF blends at the weight ratios at 40/60 1 wt% of CB. It was observed that the curve of first run was similar to those of second, fifth, tenth, and twentieth run. The transition temperature regions of PI/PSF/CB composites was observed at about 180-210°C, where the volume resistivity changed by 2 orders of magnitude. Furthermore, the change of PTC transition temperature was not obviously observed in the heating cycles greater than 5 times.

5.9 Selective Distribution of CB Particles into PI/PSF Blends

Recently, one promising method to reduce the amount of conductive fillers in composites is to use immiscible or partially miscible polymer blends. The selective localization of CB in one of the phases of the polymer blend is a very efficient strategy to decrease the CB percolation threshold. The phenomenon is known as a double percolation behavior [53, 68]. The selective localization of CB depends on surface tension, viscosity, degree of crystallinity of components and process of polymer blends [53] as follows:

- CB particles selectively locate in one of two polymer phases where a lower CB interfacial tension between polymer and CB is obtained that is predicted by Young's equation.
- The percolation threshold of semi-crystalline polymer are lower than amorphous polymer due to CB is unable to penetrate the crystalline regions, they are preferentially isolated entirely in the amorphous region. Thus, CB particles prefer to accumulate in the amorphous than semi-crystalline polymer.
- When the polymer components exhibit different viscosities. CB is found to accumulate in the polymer component with the lower viscosity during processing. For PI/PSF blend, are expected to be selectively located in PI phase because 1) the interfacial tension between PI and CB ($\gamma_{PI\text{-}CB}$ = 5.7 mJ/m^2) is lower than PSF and CB ($\gamma_{PI\text{-}CB}$ = 13.0 mJ/m^2) [69]. 2) PSF has more crystallinity than PI therefore the penetration of CB into PI phase tends to be more than PSF. Finally the difficult viscosity of PI used is lower than PSF. From those three reasons, it is very likely that the CB particles should be presented in the PI phase than in the PSF phase. To elucidate the selective localization of the CB in the PI/PSF blends, the optical microscope of CB-filled PI/PSF blends has been performed as shown in Figure 5.12a-5.12c.

Figure 5.12a shows CB particles which were used as conductive filler in PI, PSF, and PI/PSF blends. The micrographs revealed relatively good distribution of CB in both PI

and PSF homopolymer with the observed aggregate size to be in the range of 0.3-1 μm. Note that CB aggregates are visualized as bright aggregate in the micrograph even though the whole surface were coated with a thin layer of gold. Additionally, the different distribution of CB in PI domains as well in PSF as CB domains in PI/PSF blend at a fixed blend ratio of 40/60 with 1 wt% CB can be evidently observed in Figure 5.12c. This selective distribution of CB in the PI phase is attributed to its lower interfacial free energy, crystallinity, and viscosity compared to PSF phase as discussed above.

5.10 Morphology of CB-Filled PI/PSF Blends

Figure 5.13a-5.13b show the freeze fracture surface of CB-filled PI/PSF blends at the weight ratios inclusive 100/0, 40/60 with CB as conductive at a fixed CB content of 1 wt%. The result from microscope illustrated the preferential localization of CB in the PI phase. The discrete domains of selective distribution CB in the PI phase into PSF matrix were observed in PI/PSF blends with domain shape changing from more spherical shape to oval or more elongated shape with increasing fraction of PSF Furthermore, For the CB filled PI/PSF blends of 40/60 (Figure 5.13b), the increase in the PSF at about this high contents resulted in the formation of PSF continuous structure as seen in the figure. It is clearly seen that without CB, the co-continuous structure will occur at the PSF content about 60 wt% in PI whereas with the presence of CB (1 wt%). At this point, both PI domains as well as CB particles in well the PI domains formed continuous structures, which are known as a double percolative structures that can reduce the percolation threshold of the CB used.

According to Paul and Barlow relation [36], Equation (5.3), which gives a general trend for co continuity formation based on blend components relative viscosities, introducing CB into PI phase increased the PSF phase viscosity and consequently increased the volume fraction required to achieve co-continuity. Existence of CB in

one phase of blend matrix is postulated to increase the friction between the major phase and dispersed phase. Such increase of friction could lead some deformations producing elongated dispersed morphologies [55].

5.11 Effect of Processing Sequence on the Electrical Properties

In this work, the effect of different processing sequence on the electrical properties was investigated. In addition to the simultaneously mixtures of PI+PSF+CB, (PI+CB)/PSF, (PSF+CB)/PP and (PP+PSF)/CB blends were the compounds prepared by pre-blending CB with PI (or PSF) followed by the addition of PSF (or PI) or blending PI with PSF followed by the addition of CB. Table 5.4 shows the volume resistivity of 1 wt% CB-fitted PI/PSF blend ratio of 60/40, the volume resistivity of the simultaneously blended, (PI+PSF)/CB and the (PI+CB)/PSF samples is about the same (0.3-4.4x10^4 Ω cm). While the volume resistivity of the (PI+CB)/(PSF+CB) and the (PSF+CB)/PI sample is higher (i.e. 0.6-1.4x10^6 Ω cm) For the (PI+CB)/PSF composite, CB preferentially localizes in the PI phase, as in the simultaneous blended and (PI+PSF)/CB samples. The migration of CB from the PI phase to PSF rarely occurs because of the better affinity between PI and CB than PSF and CB. However, the addition of PI into PSF/CB caused the migration of CB from the PSF domains to the PI domains, reducing the CB concentration in the continuous PSF matrix, thus resulted in an increase in the volume resistivity of the specimen. The trend of CB to preferentially migrate from PSF to PI phases is probably due to the lower viscosity of PI at the processing temperature and the lower interfacial surface tension of PI and CB compared to PSF and CB similar behavior was also reported in PI/PEEK/CB composite by Gao et al. [55].

5.12 Tensile Properties of CB-Filled PI/PSF Blends

Figures 5.14-5.16 show tensile properties of PI/PSF blends at weight ratios at 40/60 with CB as conductive filler ranging from 0 to 5 wt%. Tensile moduli of PI/PSF

blends at weight ratios at 40/60 as a function of CB content are plotted in Figure 5.14. As the CB content increased, an increase in the modulus value or the brittleness was observed. The tensile modulus increased with increasing CB content as expected since CB is stiffer than PI and PSF. Similar enhancement in stiffness was observed for other polymers reinforced by CB [55, 70]. Additionally, the tensile modulus of PI/PSF/CB composites expectedly decreased with increasing PSF fraction due to the introduction of the softer elastomeric content into the blends. Similar behavior was also observed by Cao et al. in the case of PEEK blended with PI having CB as a conductive filler [55].

Tensile strength values of PI/PSF/CB composites were shown in Figure 5.15. The tensile strength of the composites at PI/PSF blend ratios at 40/60 was observed to slightly decrease with increasing CB content. The tensile strength values were also found to slightly decrease with greater CB contents of 1-5 wt%. As shown in this figure, the tensile strength values of the PI/PSF/CB composites were found to decreases with increasing CB content. It is postulated that the aggregation and agglomeration may present in the CB thus cause some defects in the composites resulting in lowering of the tensile strength values. These observed phenomena are often observed in CB-filled systems e.g. CNT-PI [66], and CNT-PSF [67]. Moreover, the tensile strength for PI/PSF/CB composites was found to increase with increasing PSF content as well. Despite the reduced tensile strength, all the tensile strength values of our PI/PSF/CB composites were still much higher than that of commercial products (i.e. > 35 MPa) [33].

Elongation at break of PI/PSF/CB composites is shown in Figure 5.16. It is clearly seen that an increase in the CB particles tended to lower the elongation at break of the resulting composites. That means the toughness of composites was reduced. In addition, the values of elongation at break for the PI/PSF/CB composites were slightly higher than those of PI/CB composites due to the ductile effect of the PSF.

5.13 Thermogravimetric Anatysis (TGA) of CB-Filled PI/PSF Blend

TGA thermograms under nitrogen of PI/PSF blend at a fixed blend ratio of 40/60 with CB as conductive filler ranging from 0 to 5 wt% are shown in Figure 5.16. The corresponding numerical results were summarized in Table 5.5. The temperatures corresponding to 5 % weight loss ($T_{5wt\%}$) are essential to evaluate the decomposition of PI/PSF/CB composites on onset stage. $T_{5wt\%}$ was found to increase with the increase of CB content as seen in the Figure 5.17. It is apparent that thermal decomposition temperature at $T_{5wt\%}$ for PI/PSF/CB composites shifted significantly to a higher temperature range than that of the neat PI/PSF blend, which indicated an improvement of thermal stability of the polymeric matrix due to the presence of the CB filler. Therefore, PI/PSF blend ratio of 60/40 with 5 wt% CB (maximum content in this system) exhibited the highest $T_{5wt\%}$ (512°C), which was shifted approximately 8°C towards high temperature compared to that of the neat PI/PSF blend. This substantial enhancement in the thermal properties of the CB-filler PI/PSF blend was likely due to the barrier effect of CB in the composites [71]. The degradation temperature tended to increase with increasing the amount of the conductive filter in the polymer matrix had been observed in the systems of CB particles filled-PI composites [72].

The relationship between CB contents and residual char of the PI/PSF/CB composites is also illustrated in Figure 5.17 and the corresponding numerical values listed in Table 5.5. CB filler exhibited very high thermal stability thus the composite did not experience any significant weight loss within the temperature range of 30-900°C under the TGA investigation [72]. When the temperature was raised to 900°C, mainly the PI/PSF fraction was decomposed thermally and formed char. Therefore, the amounts of char residue in this case could be approximated to correspond directly to the content of the CB filler and char residue of the PI/PSF fraction.

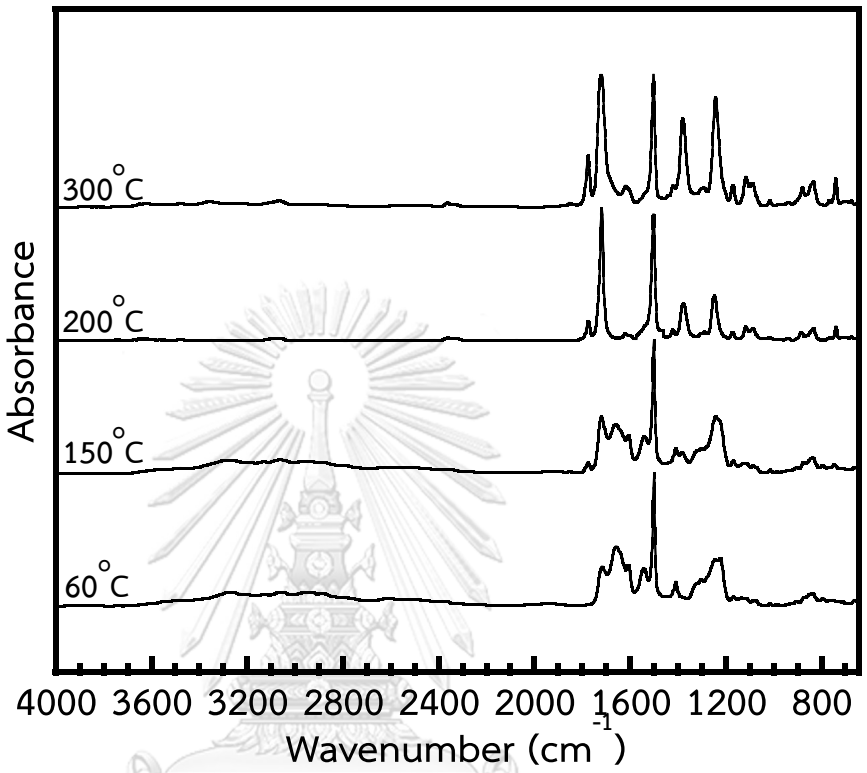

Figure 5.1: FTIR spectra of *s*-BPDA/ODA polyimide films prepared at 60°C for 8 hours and 150, 200, and 300°C (1 hour for each temperature).

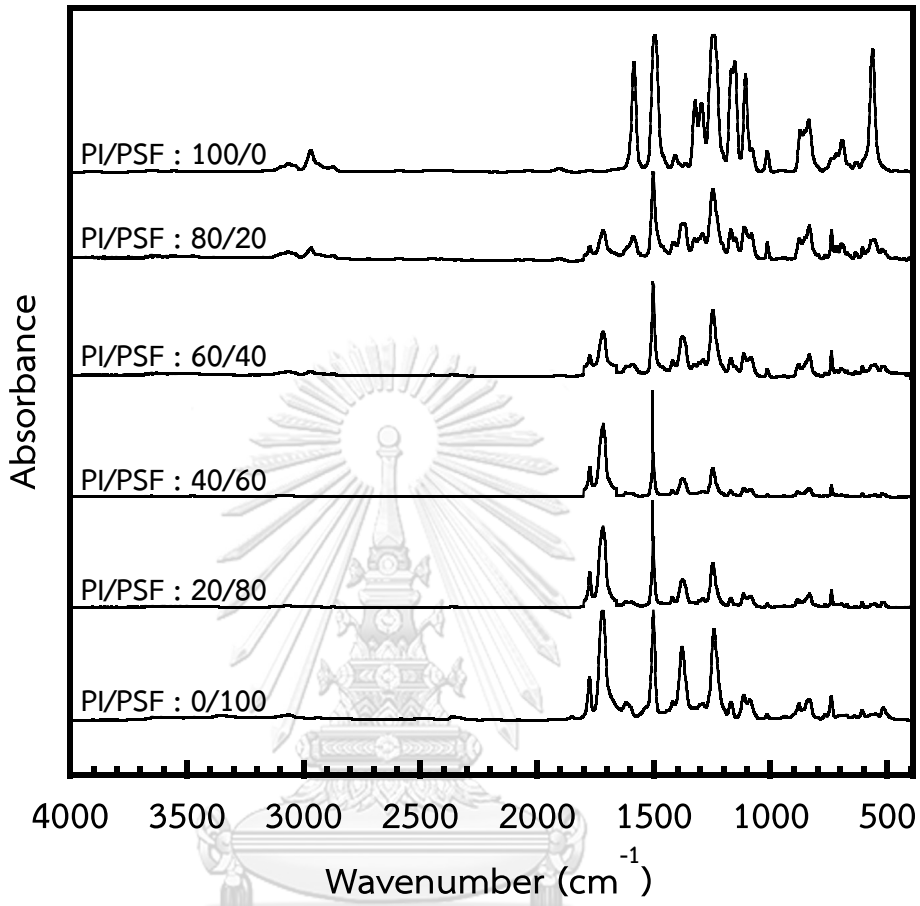

Figure 5.2: FTIR spectra of *s*-BPDA/ODA polyimide at various PSF contents: PSF, 80 wt% PSF, 60 wt% PSF, 40 wt% PSF, and *s*-BPDA/ODA polyimide.

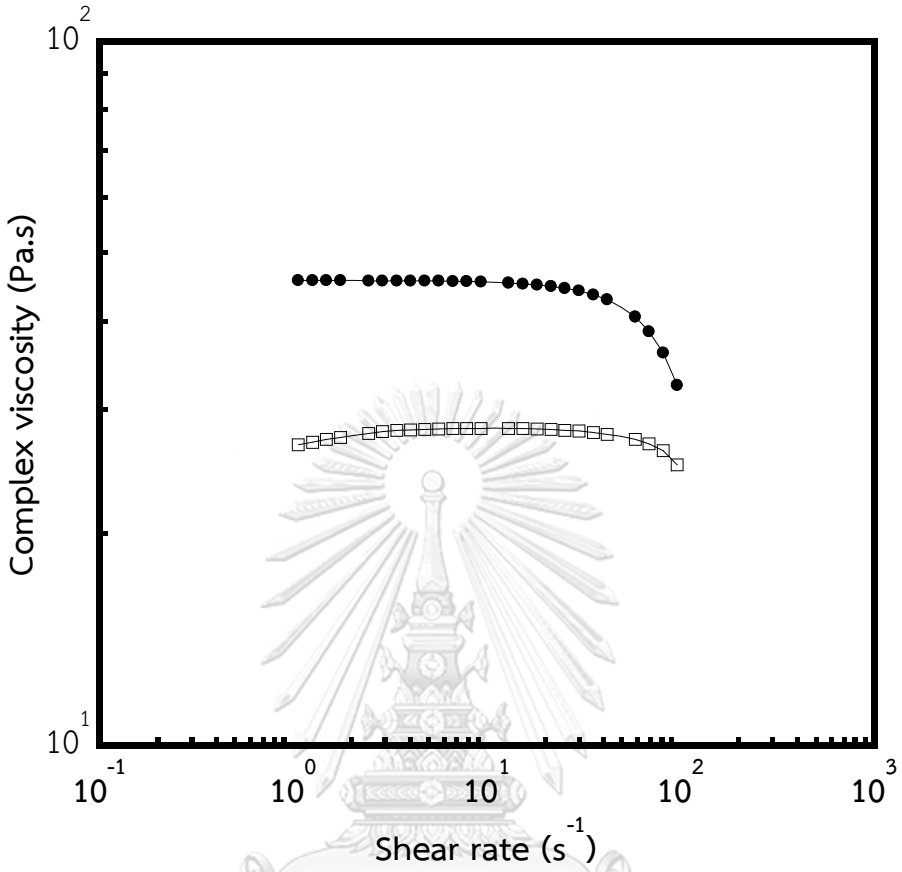

Figure 5.3: Shear rate dependence of viscosity at 30°C: (●) PSF, (□) PI.

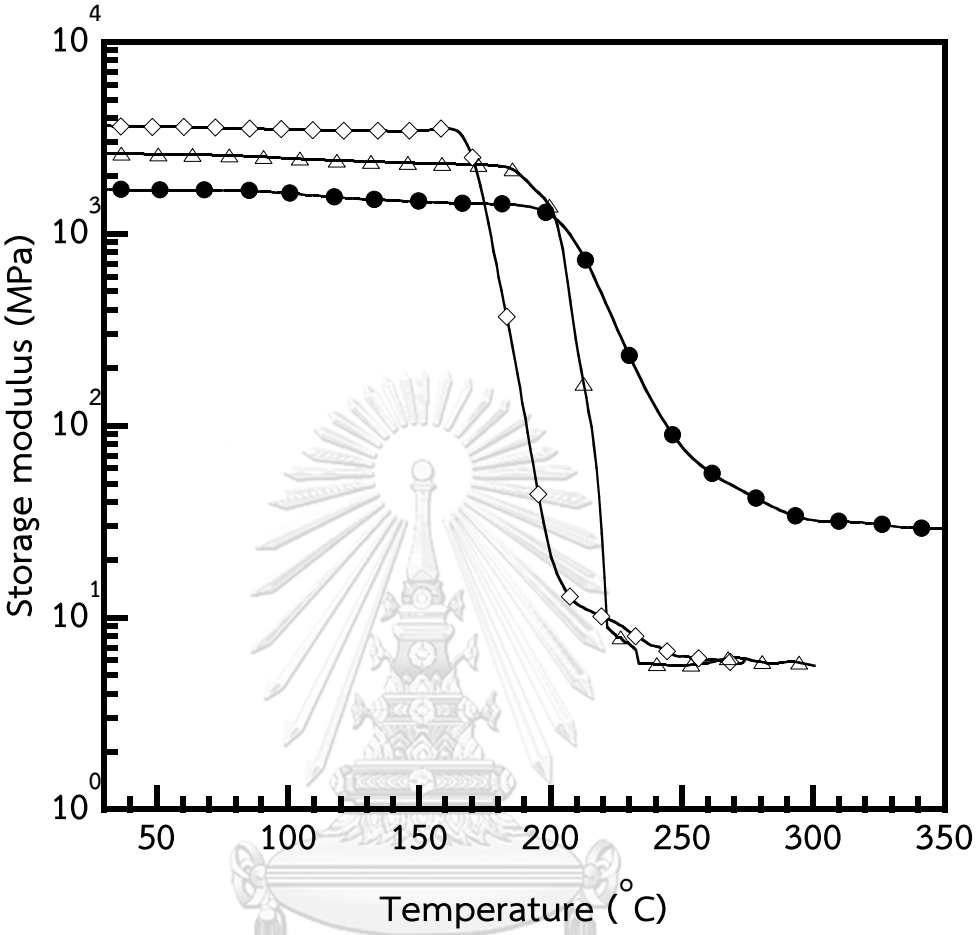

Figure 5.4: Storage modulus versus temperature of PI/PSF blends at various blend ratios: (●) 0/100, (△) 40/60, and (◇) 100/0.

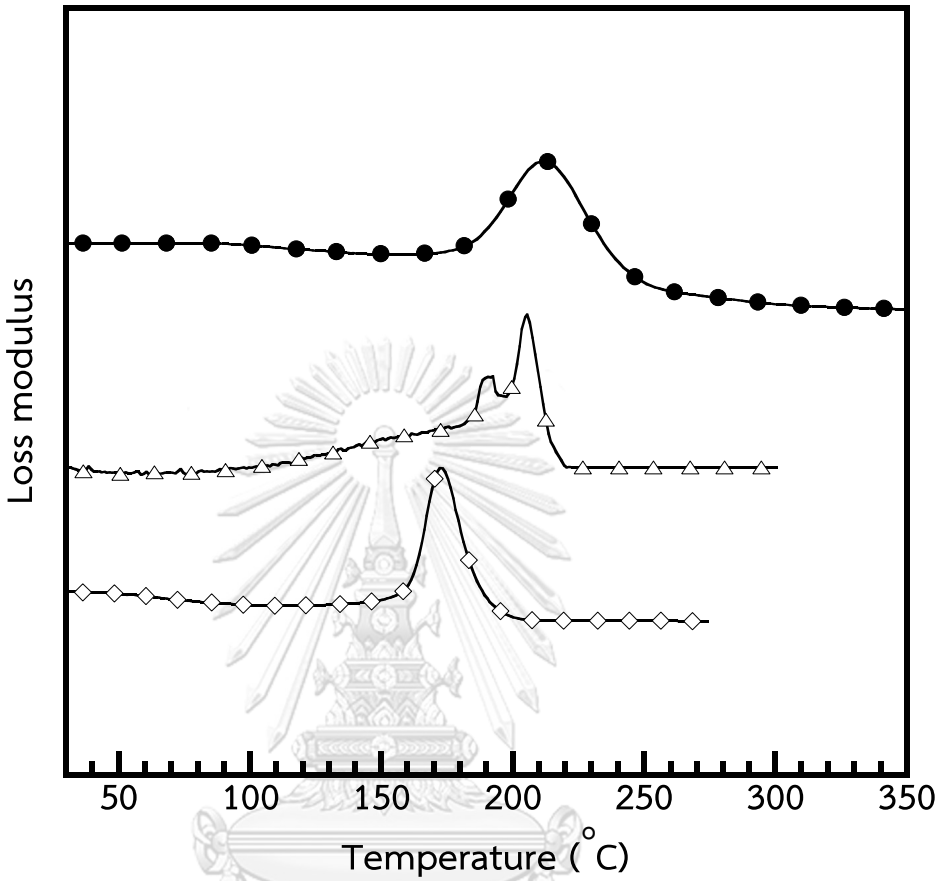

Figure 5.5: Loss modulus versus temperature of PI/PSF blends at various blend ratios: (●) 100/0, (△) 40/60, and (◇) 0/100.

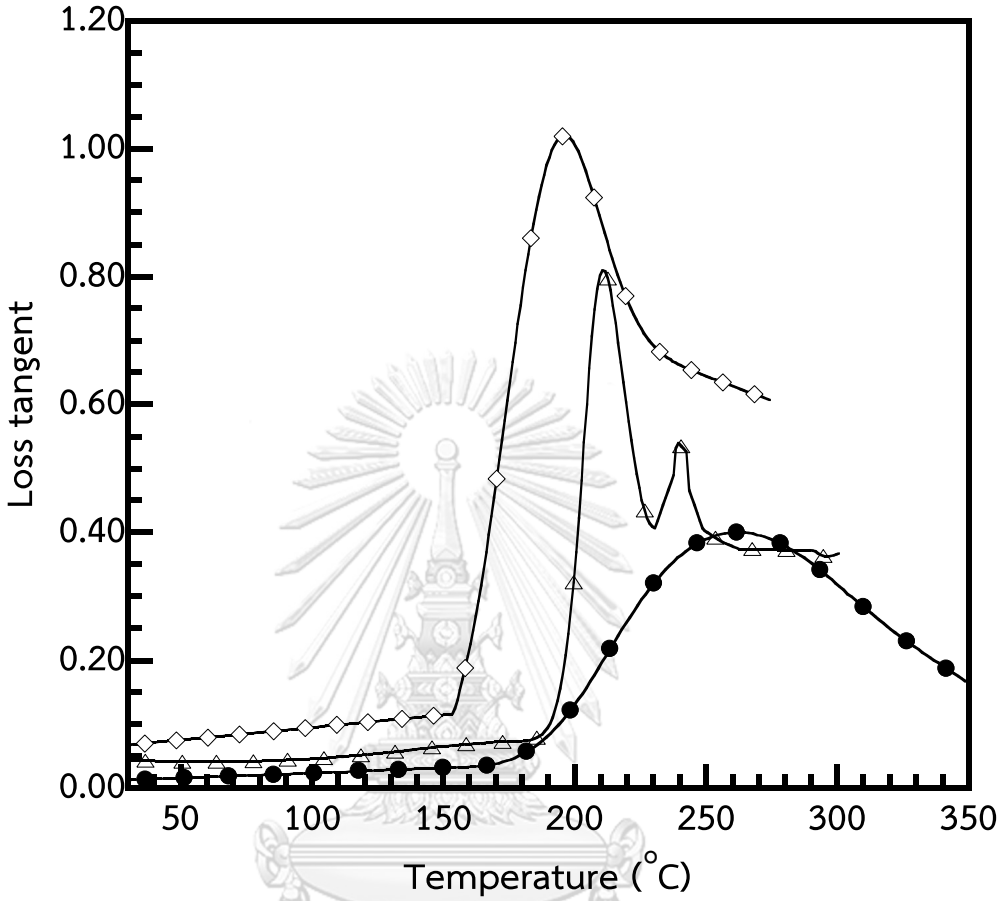

Figure 5.6: Loss tangent versus temperature of PI/PSF blends at various blend ratios: (●) 100/0, (△) 40/60, and (◇) 0/100.

Table 5.1: Glass transition temperature of PI/PSF blends at various blend ratios from loss modulus curves.

PI/PSF blend ratio	T_g(°C)	
	T_{g1}	T_{g2}
100/0	-	212
40/60	191	205
0/100	172	-

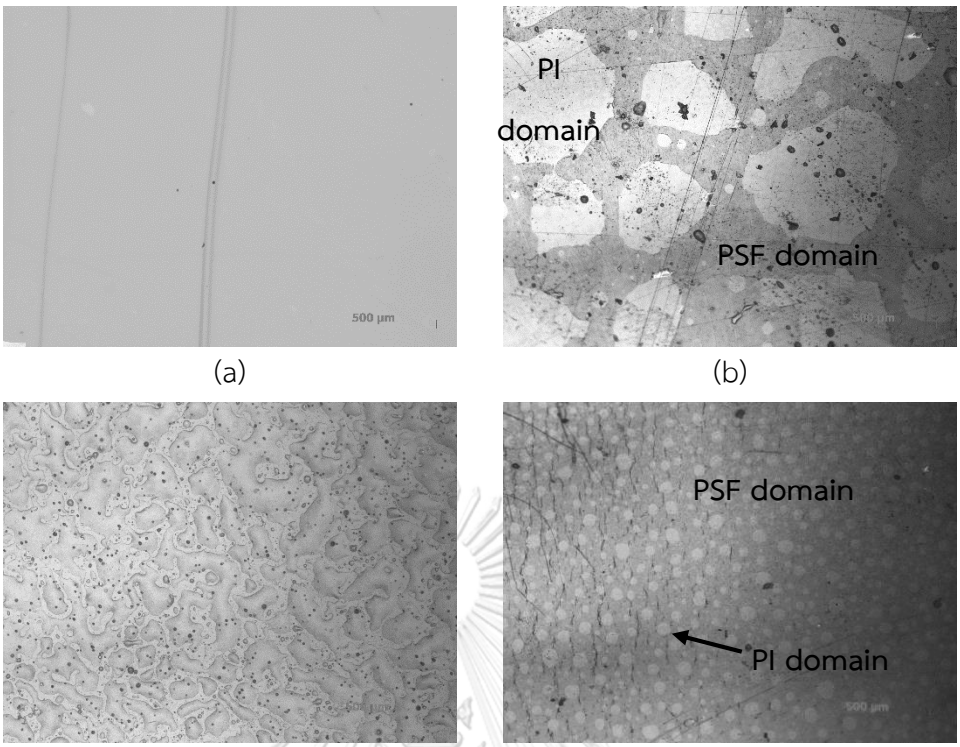

Figure 5.7: OM micrographs of PI/PF blend at various blend ratios: (a) 100/0, (b) 50/50, (c) 40/60, and (d) 30/70.

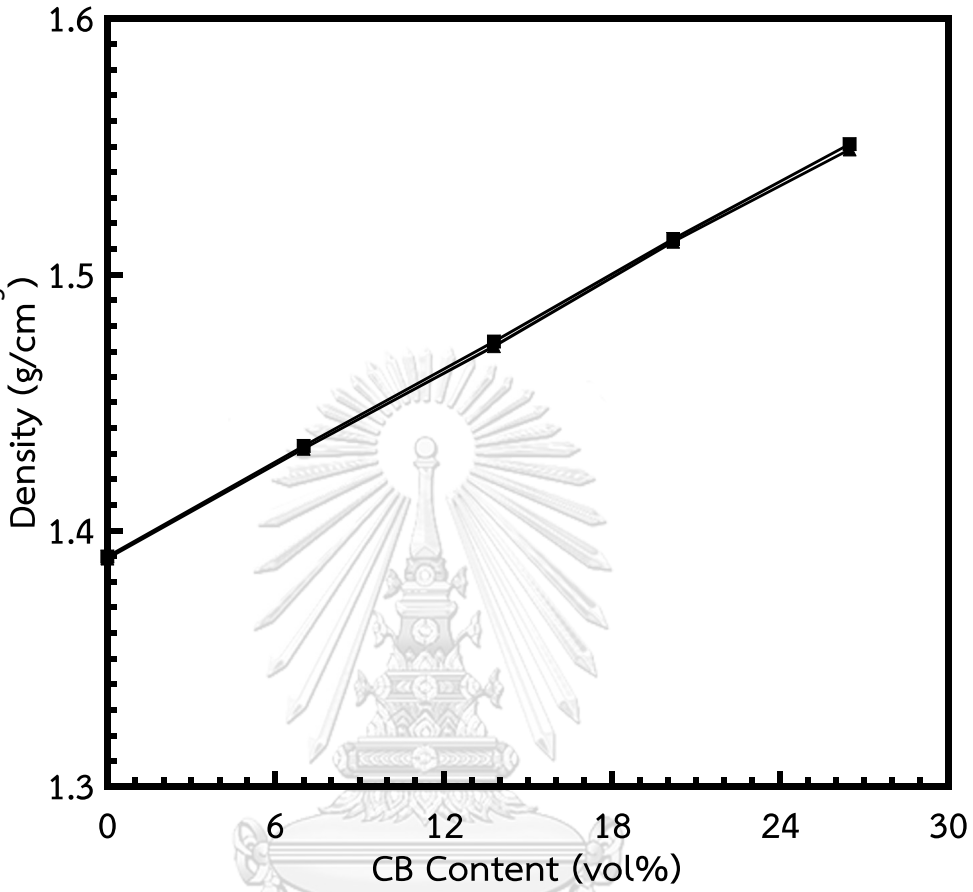

Figure 5.8: Density versus blend ratio PI/CB composites: (▲) actual density and (■) theoretical density.

Table 5.2: Actual and theoretical densities of CB-filled PI/PSF blends at 100/0 and 40/60 ratios.

CB content (wt%)	Theoretical density (g/cm^3)		Actual density (g/cm^3)	
	100/0	40/60	100/0	40/60
0	1.390	1.304	1.389	1.302
5	1.405	1.356	1.432	1.356
10	1.421	1.406	1.472	1.405
15	1.436	1.453	1.513	1.452
20	1.451	1.497	1.549	1.496

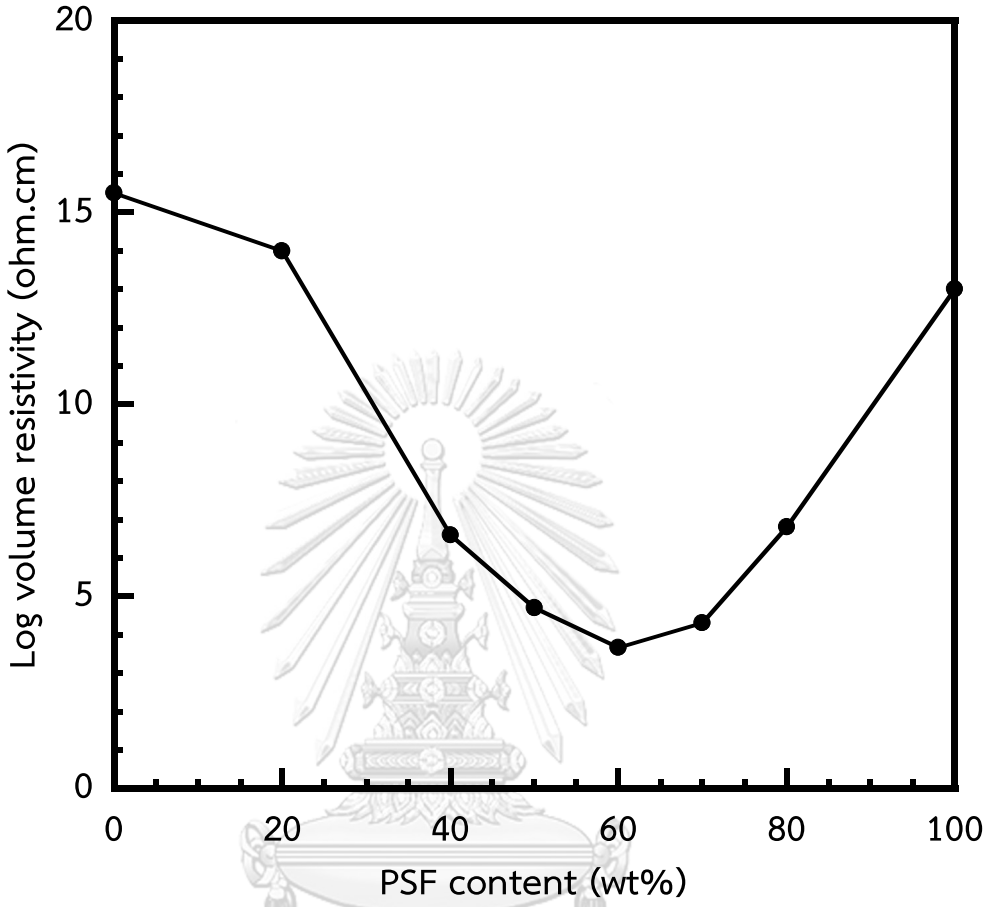

Figure 5.9: Volume resistivity of 1 wt% CB-filled PI/PSF blends at various ratios.

Table 5.3: Volume resistivity of 1 wt% CB-filled PI/PSF blend at various blend ratios.

PI/PSF blend ratio	Volume Resistivity (Ω.cm)	Log Volume Resistivity (Ω.cm)
0	3.2×10^{15}	15.5
20	1.0×10^{14}	14.0
40	4.0×10^{6}	6.6
50	5.0×10^{4}	4.7
60	5.0×10^{3}	3.7
70	1.9×10^{4}	4.3
80	6.3×10^{6}	6.8
100	1.0×10^{13}	13

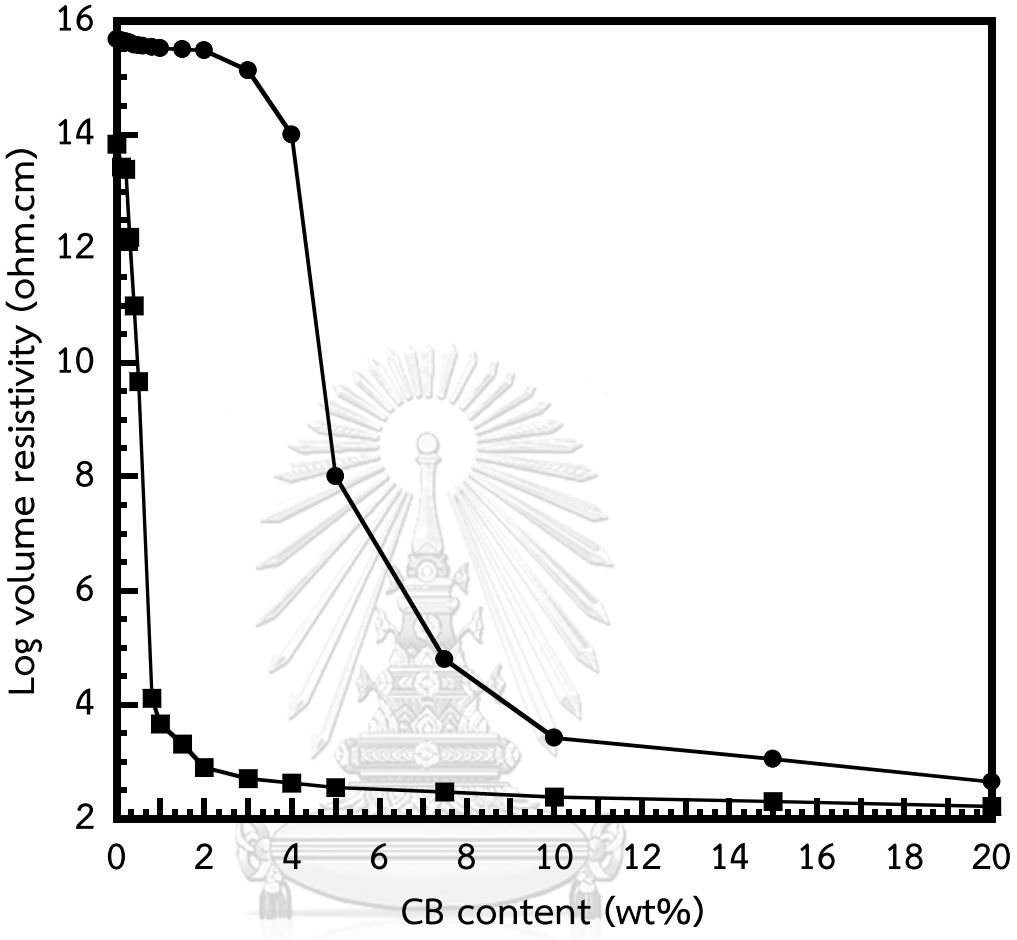

Figure 5.10: Volume resitivity of CB-filled PI and PI/PSF blends at various blend ratios: (●) 100/0, and (■) 40/60.

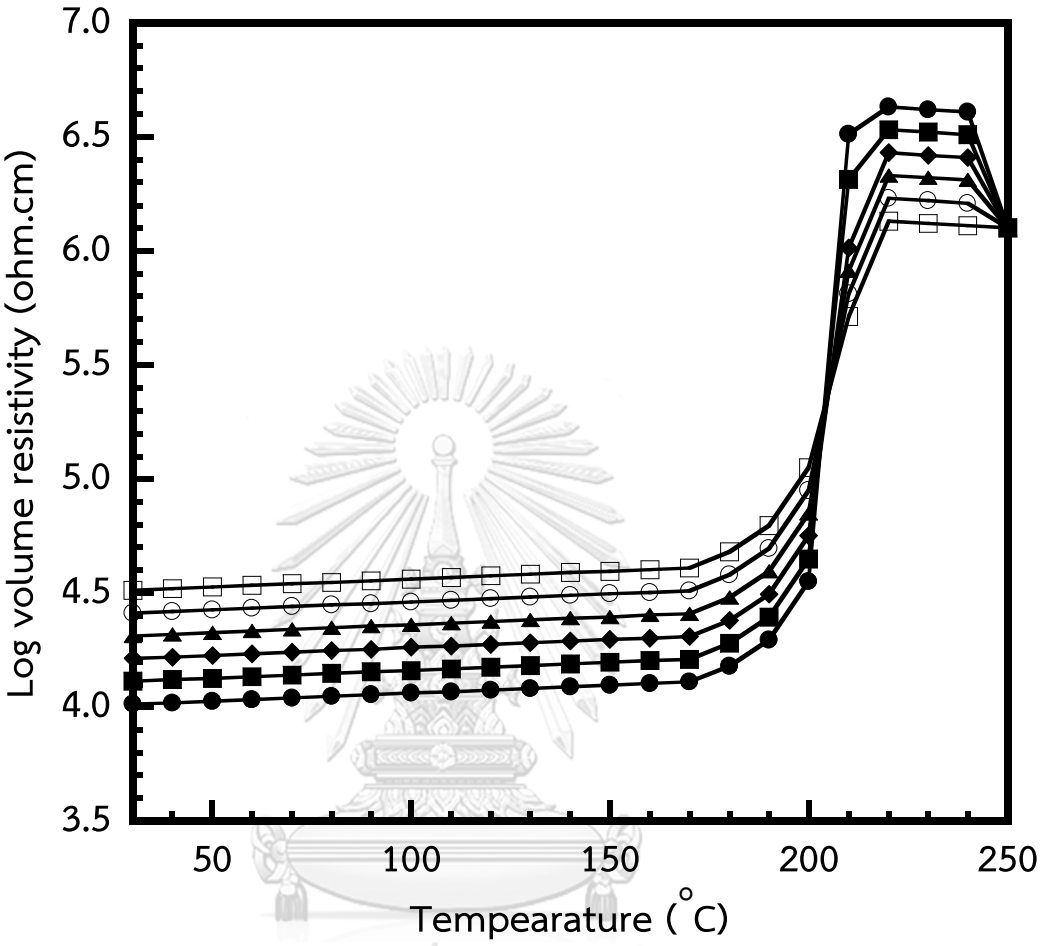

Figure 5.11: Temperature dependences of volume resistivity of CB-filled PI/PSF blend ratio (40/60) at various heating cycles: (●) 1st run, (■) 2nd run, (◆) 5th run, (▲) 10th run, (○) 15th run, and (□) 20th run.

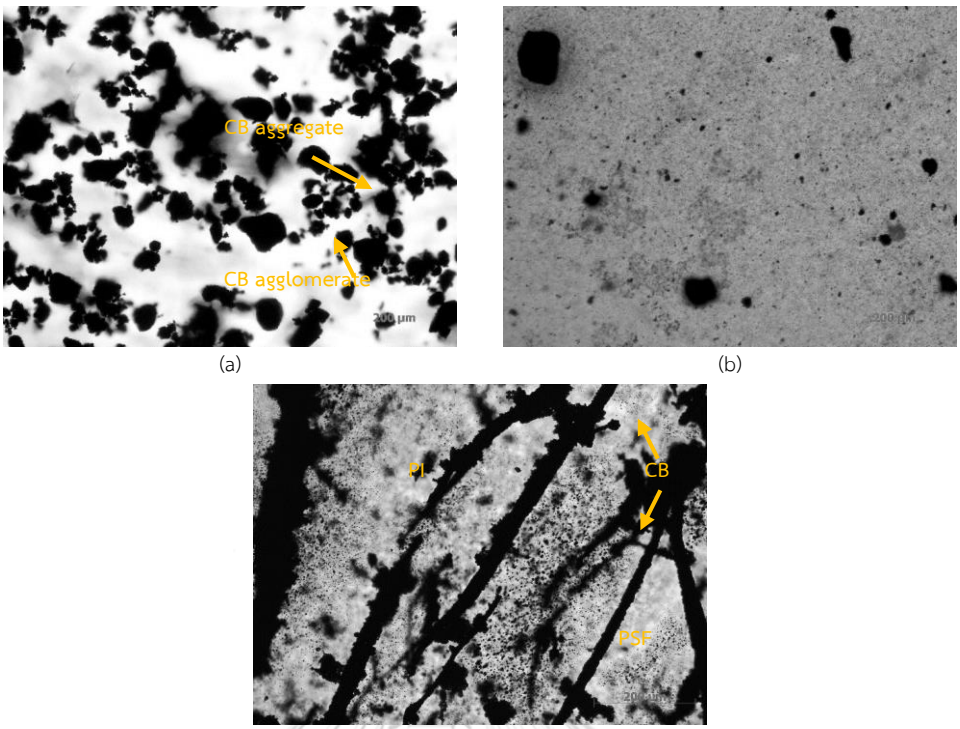

Figure 5.12: OM micrographs of CB-filled PI/PSF blends: (a) pure CB (b) 1 wt% CB-filled PI and (c) 1 wt% CB-filled PI/PSF blend ratio (40/60).

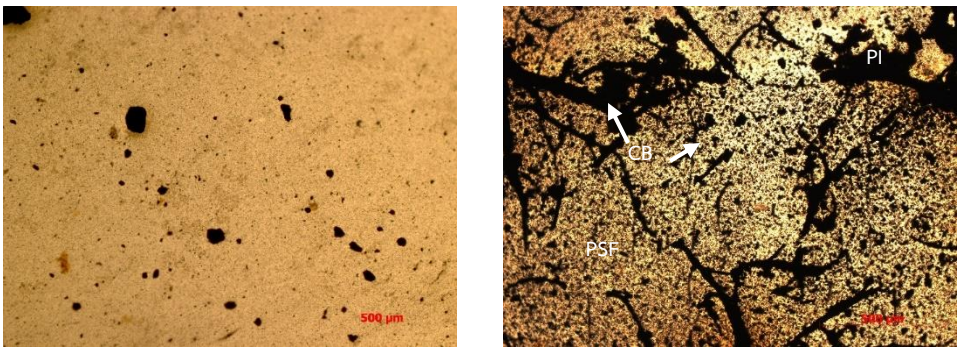

(a) (b)

Figure 5.13: OM micrographs of 1 wt% CB-filled PI/PSF blends at various blend ratios: (a) 100/0 (b) 40/60.

Table 5.4: Volume resistivity of PI/PSF/CB blends with processing sequence

Sample composition	Method of processing	Volume resistivity (Ω.cm)
40/60 PI/PSF 3 wt% CB	PI/(CB+PSF)	$(2.7\pm0.07)\times10^{3}$
	Simultaneously blended	$(2.7\pm0.17)\times10^{3}$
	(PI+PSF)/ CB	$(4.4\pm0.10)\times10^{4}$
	(PI+CB)/(PSF+CB)	$(6.2\pm0.03)\times10^{5}$
	(PSF+CB)/PI	$(1.4\pm0.07)\times10^{6}$

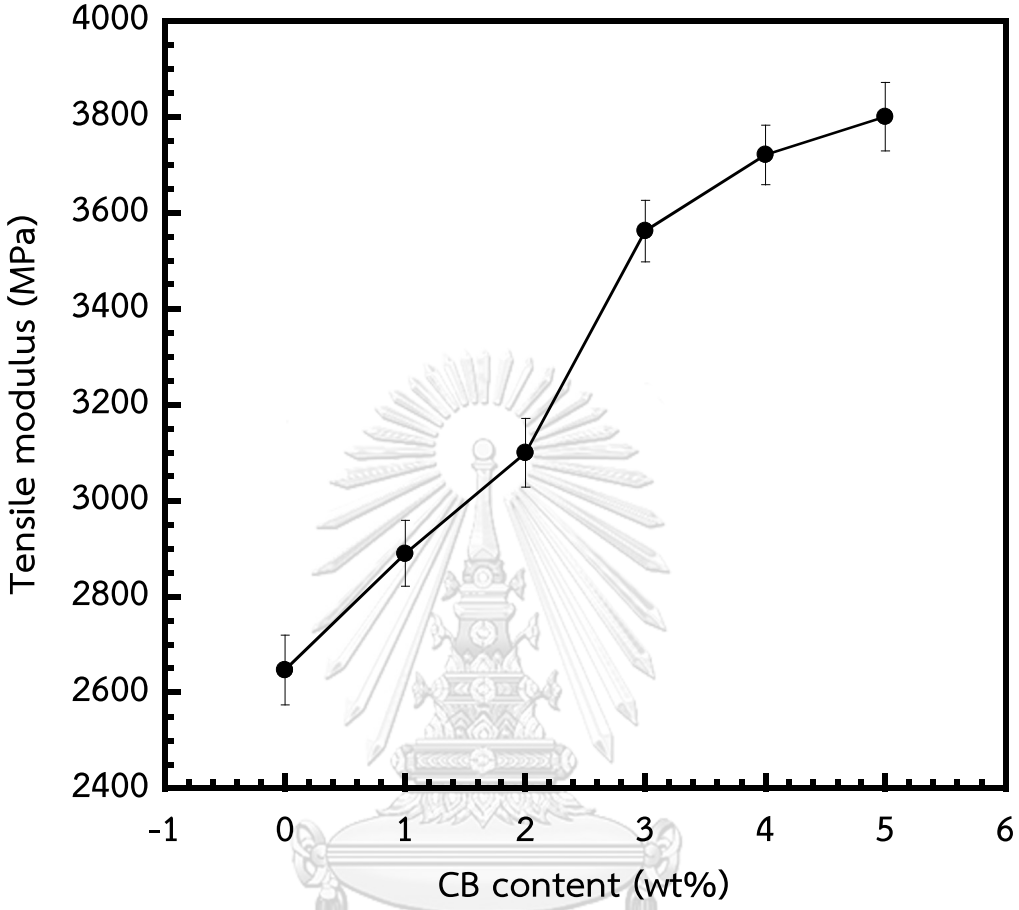

Figure 5.14: Tensile modulus of CB-filled PI/PSF blend at 40/60.

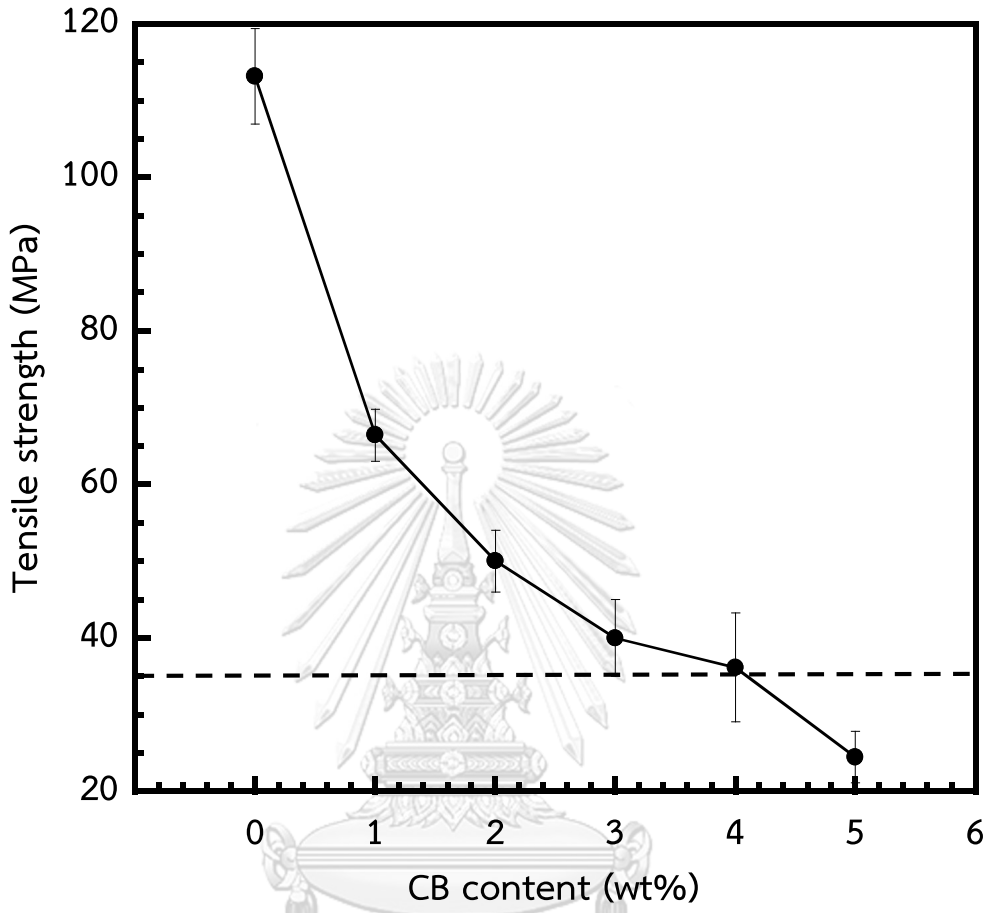

Figure 5.15: Tensile strength of CB-filled PI/PSF blend at 40/60.

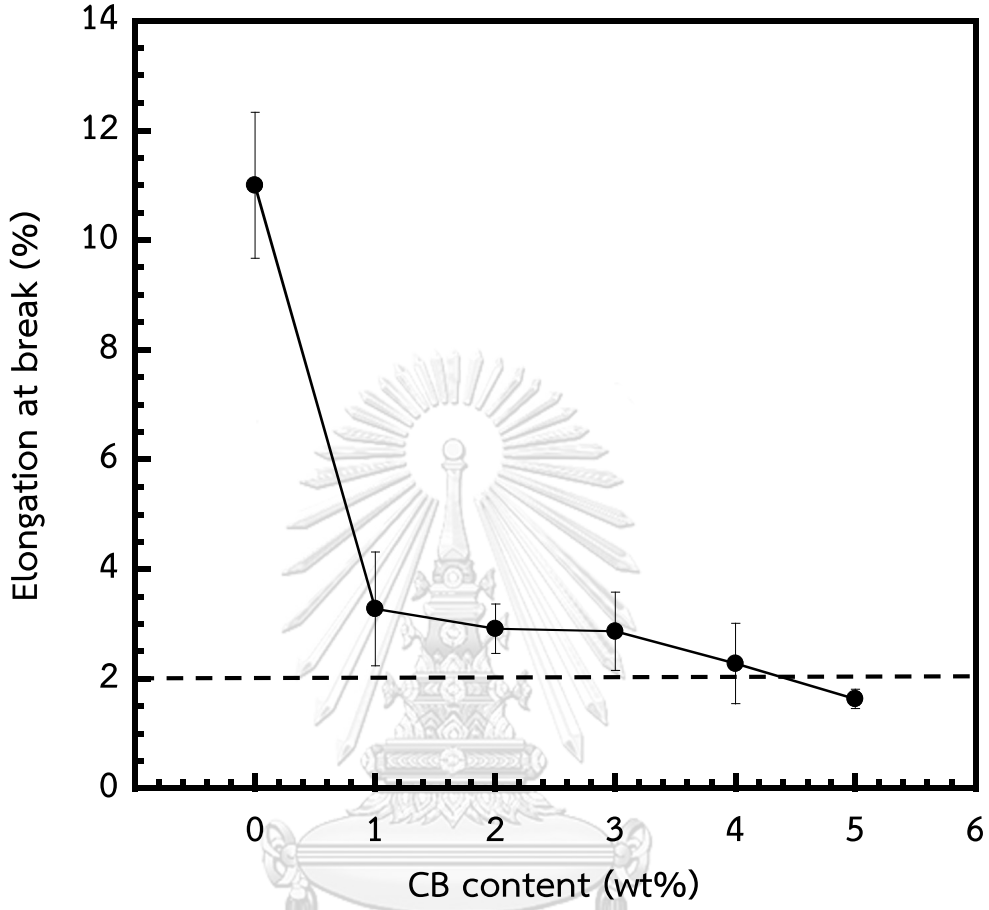

Figure 5.16: Elongation at break of CB-filled PI/PSF blend at 40/60.

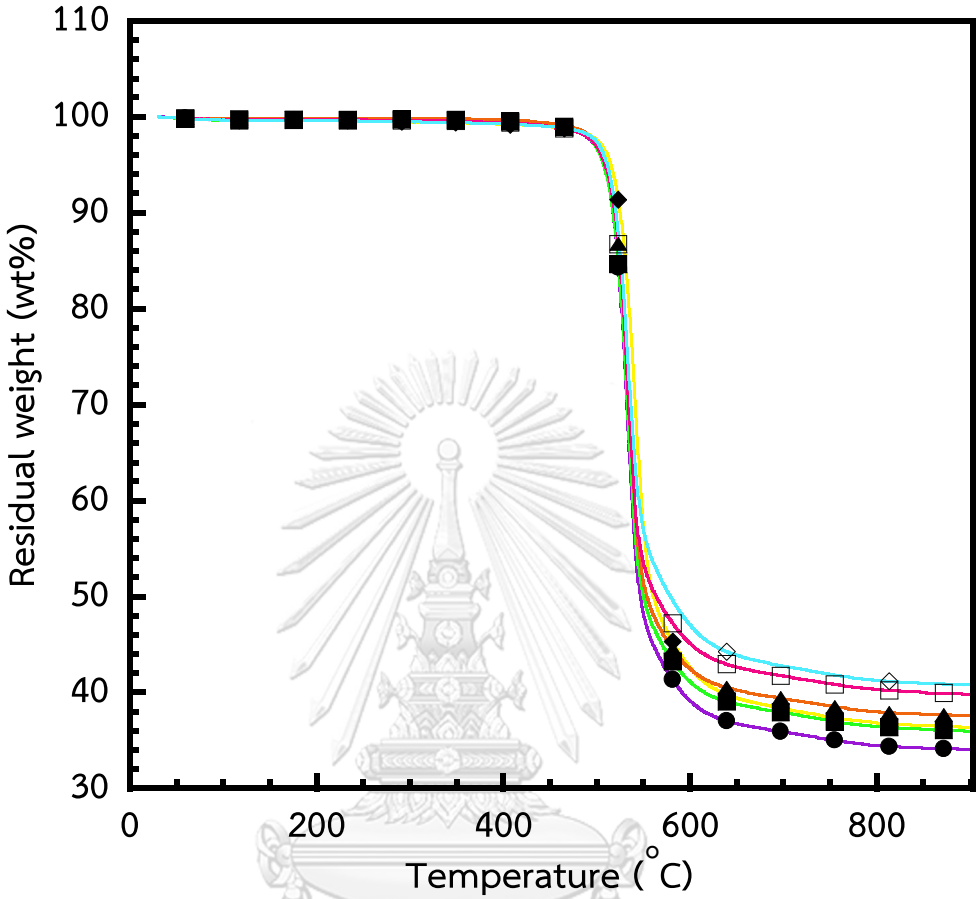

Figure 5.17: Thermogravimetric analysis (TGA) of CB-filled PI/PSF blend ratio (40/60) at various CB contents: (●) 0 wt%, (■) 1 wt%, (◆) 2 wt%, (▲) 3 wt%, (□) 4 wt% and (◇) 5 wt%.

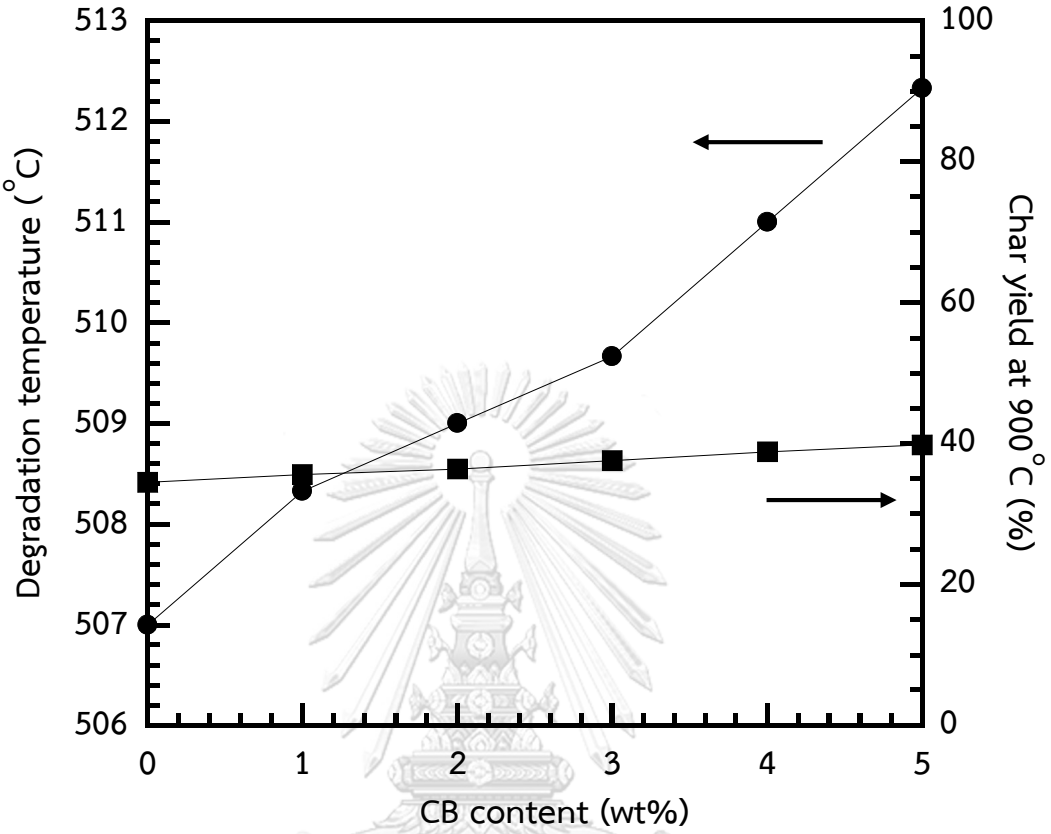

Figure 5.18: (●)Degradation temperature (5% weight loss) of CB-filled PI/PSF blend ratio of 40/60 and (■) char yield at 900°C.

Table 5.5: Degradation temperature and residual char of CB-filled PI/PSF blend ratio of 40/60 at various CB contents.

CB content (wt%)	Degradation temperature (°C) at 5% weight loss	Char yield (%) at 900°C
0	507	34.5
1	508	35.6
2	509	36.4
3	510	37.6
4	511	38.8
5	512	39.8

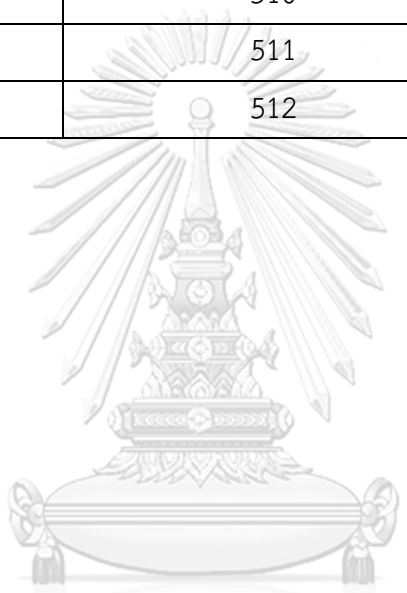

CHAPTER VI
CONCLUSION

PI/PSF blends exhibited two glass transition temperatures (T_gs) at 191 and 205°C. Both T_gs of PI and PSF phases shifted towards each other suggesting the partially miscible nature of the PI/PSF blends. The CB loading in conductive polyimide compound could be minimized through a double percolation approach. Moreover, PI/PSF blends exhibited lower percolation thresholds and greater conductivities than those of the CB-filled due to double percolation phenomena at PI/PSF ratio of 40/60 form co-continuous phase. However, percolation threshold of PI/PSF/CB composite with PI/PSF ratio of 40/60 was only about 1 wt% CB, while PI/CB composite was only about 8 wt% CB. It can be seen that the blend systems provided the lower volume resistivity value than homopolymer system. Positive temperature coefficient behavior was investigated from room temperature to 250°C, it was found that PTC threshold of PI/PSF/CB composite with PI/PSF ratio of 40/60 was about 180-210°C. In addition, the change of PTC transition temperature was not obviously observed in the heating cycles greater than 5 times. Furthermore, tensile modulus values of PI/PSF/CB composites increased with increasing CB content because the rigidity of CB was more than PI and PSF. Tensile strength and tensile elongation at break values of all PI/PSF/CB composites slightly decreased with increasing CB content due to agglomerate of CB in system. Though tensile strength and tensile elongation at break values decreased, the

values were higher than those of the commercial one. Both degradation temperature (T_d) at 5% weight loss and char yield at 900°C of all PI/PSF/CB composites were observed to increase with an increase of CB content because of thermal stability and gas barrier properties of CB. Therefore, from the results, the recommended PTC for PI compound should be 1 wt% CB-filled PI/PSF blend ratio of 40/60.

REFERENCES

1. Yang, Y., et al., *Novel carbon nanotube– polystyrene foam composites for electromagnetic interference shielding.* Nano letters, 2005. 5(11): p. 2131-2134.
2. Zhang, F., et al., *Polymer photovoltaic cells with conducting polymer anodes.* Advanced Materials, 2002. **14**(9): p. 662-665.
3. Grätzel, M., *Photoelectrochemical cells.* Nature, 2001. **414**(6861): p. 338-344.
4. Cihaner, A. and F. Algı, *A Novel Neutral State Green Polymeric Electrochromic with Superior n-and p-Doping Processes: Closer to Red-Blue-Green (RGB) Display Realization.* Advanced Functional Materials, 2008. **18**(22): p. 3583-3589.
5. Yu, M.-F., et al., *Strength and breaking mechanism of multiwalled carbon nanotubes under tensile load.* Science, 2000. **287**(5453): p. 637-640.
6. Kim, Y.J., et al., *Electrical conductivity of chemically modified multiwalled carbon nanotube/epoxy composites.* Carbon, 2005. **43**(1): p. 23-30.
7. Moisala, A., et al., *Thermal and electrical conductivity of single-and multi-walled carbon nanotube-epoxy composites.* Composites science and technology, 2006. **66**(10): p. 1285-1288.
8. Moniruzzaman, M. and K.I. Winey, *Polymer nanocomposites containing carbon nanotubes.* Macromolecules, 2006. **39**(16): p. 5194-5205.
9. Wang, H., et al., *A material with high electromagnetic radiation shielding effectiveness fabricated using multi-walled carbon nanotubes wrapped with poly (ether sulfone) in a poly (ether ether ketone) matrix.* Journal of Materials Chemistry, 2012. **22**(39): p. 21232-21237.
10. Tseng, Y.C. and E.M. Woo, *Polymer-polymer miscibility in blends of a new poly (aryl ether ketone) with poly (ether imide).* Macromolecular rapid communications, 1998. **19**(4): p. 215-218.

11. Ounaies, Z., et al., *Electrical properties of single wall carbon nanotube reinforced polyimide composites.* Composites Science and Technology, 2003. **63**(11): p. 1637-1646.
12. Gao, C., et al., *Synthesis of poly (ether ether ketone)-block-polyimide copolymer and its compatibilization for poly (ether ether ketone)/thermoplastic polyimide blends.* Polymer, 2014. **55**(1): p. 119-125.
13. Huang, J.C., *Carbon black filled conducting polymers and polymer blends.* Advances in Polymer Technology, 2002. **21**(4): p. 299-313.
14. Boyes, W., *Instrumentation reference book*. 2009: Butterworth-Heinemann.
15. Yeh, J.M., et al., *Enhanced corrosion prevention effect of polysulfone–clay nanocomposite materials prepared by solution dispersion.* Journal of applied polymer science, 2004. **92**(1): p. 631-637.
16. Monticelli, O., et al., *Preparation and properties of polysulfone–clay composite membranes.* Journal of applied polymer science, 2007. **103**(6): p. 3637-3644.
17. Musto, P., et al., *Polyimide-silica nanocomposites: spectroscopic, morphological and mechanical investigations.* Polymer, 2004. **45**(5): p. 1697-1706.
18. Wang, C., et al., *Improving the mechanical, electrical, and thermal properties of polyimide by incorporating functionalized graphene oxide.* High Performance Polymers, 2016. **28**(7): p. 800-808.
19. Al-Saleh, M.H. and U. Sundararaj, *A review of vapor grown carbon nanofiber/polymer conductive composites.* Carbon, 2009. **47**(1): p. 2-22.
20. Tang, H., et al., *Studies on the electrical conductivity of carbon black filled polymers.* Journal of applied polymer science, 1996. **59**(3): p. 383-387.
21. Gkourmpis, T., et al., *Improved electrical and flow properties of conductive polyolefin blends: Modification of poly (ethylene vinyl acetate) copolymer/carbon black with ethylene–propylene copolymer.* European Polymer Journal, 2013. **49**(8): p. 1975-1983.
22. Levon, K., A. Margolina, and A.Z. Patashinsky, *Multiple percolation in conducting polymer blends.* Macromolecules, 1993. **26**(15): p. 4061-4063.

23. Mallette, J.G., et al., *Carbon black-filled PET/HDPE blends: Effect of the CB structure on rheological and electric properties.* Journal of applied polymer science, 2001. **81**(3): p. 562-569.
24. Wu, G., B. Li, and J. Jiang, *Carbon black self-networking induced co-continuity of immiscible polymer blends.* Polymer, 2010. **51**(9): p. 2077-2083.
25. Al-Saleh, M.H. and U. Sundararaj, *Nanostructured carbon black filled polypropylene/polystyrene blends containing styrene–butadiene–styrene copolymer: Influence of morphology on electrical resistivity.* European Polymer Journal, 2008. **44**(7): p. 1931-1939.
26. Farshidfar, A., V. Haddadi-Asl, and H. Nazokdast, *Electrical and mechanical properties of conducive carbon black/polyolefin composites mixed with carbon fiber.* Journal of ASTM International, 2006. **3**(10): p. 1-8.
27. Shen, L., et al., *The combined effects of carbon black and carbon fiber on the electrical properties of composites based on polyethylene or polyethylene/polypropylene blend.* Polymer Testing, 2011. **30**(4): p. 442-448.
28. Mekhilef, N. and H. Verhoogt, *Phase inversion and dual-phase continuity in polymer blends: theoretical predictions and experimental results.* Polymer, 1996. **37**(18): p. 4069-4077.
29. Company, E.A.A.T.G., *PTC Thermistors*, in *EPCOS AG 2016*. 2016: Germany.
30. Murata Manufacturing Co., L., *PTC Thermistors (POSISTOR®)*. 2016.
31. Shanghai Xinye Electronic Co., L., *PTC heating element*. 2016.
32. Baiatu, T., *PTC thermistor and a current limiter device having at least one PTC thermistor*. 2000, Google Patents.
33. Mercx, F.P.M. and S. Ter Horst, *Positive temperature coefficient materials with reduced negative temperature coefficient effect*. 2013, Google Patents.
34. Ravati, S. and B.D. Favis, *Morphological states for a ternary polymer blend demonstrating complete wetting.* Polymer, 2010. **51**(20): p. 4547-4561.
35. Avgeropoulos, G., et al., *Heterogeneous blends of polymers. Rheology and morphology.* Rubber Chemistry and Technology, 1976. **49**(1): p. 93-104.
36. Paul, D. and J. Barlow, *Polymer blends.* Journal of Macromolecular Science—Reviews in Macromolecular Chemistry, 1980. **18**(1): p. 109-168.

37. Accorsi, J.V., *The impact of carbon black morphology and dispersion on the weatherability of polyethylene.* KAUTSCHUK UND GUMMI KUNSTSTOFFE, 2001. **54**(6): p. 321-326.

38. Leblanc, J.L., *Filled polymers: science and industrial applications*. 2009: CRC Press.

39. Al-Saleh, M.H. and U. Sundararaj, *An innovative method to reduce percolation threshold of carbon black filled immiscible polymer blends.* Composites Part A: Applied Science and Manufacturing, 2008. **39**(2): p. 284-293.

40. Hussain, M., Y.-H. Choa, and K. Niihara, *Fabrication process and electrical behavior of novel pressure-sensitive composites.* Composites Part A: applied science and manufacturing, 2001. **32**(12): p. 1689-1696.

41. Mamunya, Y. *Polymer blends filled with carbon black: structure and electrical properties*. in *Macromolecular Symposia*. 2001. Wiley Online Library.

42. Badesha, S.S. and J.A. Swift, *Practical surfaces: beyond the wheel.* Surface science, 2002. **500**(1): p. 1024-1041.

43. Mamunya, Y.P., et al., *Percolation phenomena in polymers containing dispersed iron.* Polymer Engineering & Science, 2002. **42**(1): p. 90-100.

44. Feng, J., C.m. Chan, and J.x. Li, *A method to control the dispersion of carbon black in an immiscible polymer blend.* Polymer Engineering & Science, 2003. **43**(5): p. 1058-1063.

45. Fenouillot, F., P. Cassagnau, and J.-C. Majesté, *Uneven distribution of nanoparticles in immiscible fluids: morphology development in polymer blends.* Polymer, 2009. **50**(6): p. 1333-1350.

46. Wu, S., *Interfacial and surface tensions of polymers.* Journal of Macromolecular Science—Reviews in Macromolecular Chemistry, 1974. **10**(1): p. 1-73.

47. Cheah, K., M. Forsyth, and G. Simon, *Processing and morphological development of carbon black filled conducting blends using a binary host of*

poly (styrene co-acrylonitrile) and poly (styrene). Journal of Polymer Science Part B: Polymer Physics, 2000. **38**(23): p. 3106-3119.

48. Cui, L., et al., *Electrical properties and conductive mechanisms of immiscible polypropylene/Novolac blends filled with carbon black.* European Polymer Journal, 2007. **43**(12): p. 5097-5106.
49. Kapantaidakis, G., et al., *Interrelation between phase state and gas permeation in polysulfone/polyimide blend membranes.* Journal of Polymer Science-B-Polymer Physics Edition, 1999. **37**(19): p. 2788-2798.
50. Ammar, A.M., *The Morphology and Mechanical Properties of Polysulfone/Polyimide Nanocomposite Films*. 2012, University of Akron.
51. Linares, A. and R. Benavente, *Effect of sulfonation on thermal, mechanical, and electrical properties of blends based on polysulfones.* Polymer journal, 2009. **41**(5): p. 407-415.
52. Felisberti, M.-I., L.L. de Lucca Freitas, and R. Stadler, *Mechanical relaxation in miscible polymer systems: the glass transition regime in poly (vinylmethylether)(PVME)-cross-polystyrene (PS) semi-interpenetrating networks.* Polymer, 1990. **31**(8): p. 1441-1448.
53. Gao, C., et al., *High-performance conductive materials based on the selective location of carbon black in poly(ether ether ketone)/polyimide matrix.* Composites Part B: Engineering, 2015. **79**(Supplement C): p. 124-131.
54. Liang, K., et al., *Thermal and rheological properties of miscible polyethersulfone/polyimide blends.* Journal of Polymer Science Part B: Polymer Physics, 1992. **30**(5): p. 465-476.
55. Gao, C., et al., *High-performance conductive materials based on the selective location of carbon black in poly (ether ether ketone)/polyimide matrix.* Composites Part B: Engineering, 2015. **79**: p. 124-131.
56. Ku, H., et al., *A review on the tensile properties of natural fiber reinforced polymer composites.* Composites Part B: Engineering, 2011. **42**(4): p. 856-873.
57. Fu, S.-Y., et al., *Effects of particle size, particle/matrix interface adhesion and particle loading on mechanical properties of particulate–polymer composites.* Composites Part B: Engineering, 2008. **39**(6): p. 933-961.

58. Zhang, X., et al., *Two-step positive temperature coefficient effect with favorable reproducibility achieved by specific "island-bridge" electrical conductive networks in HDPE/PVDF/CNF composite.* Composites Part A: Applied Science and Manufacturing, 2017. **94**: p. 21-31.

59. Gardner II, S.H., *An investigation of the structure-property relationships for high performance thermoplastic matrix, carbon fiber composites with a tailored polyimide interphase*. 1998.

60. Nah, C., et al., *Intercalation behavior of polyimide/organoclay nanocomposites during thermal imidization.* Composites Part B: Engineering, 2004. **35**(2): p. 125-131.

61. Yang, C.-P. and Y.-Y. Su, *Colorless polyimides from 2, 3, 3′, 4′-biphenyltetracarboxylic dianhydride (α-BPDA) and various aromatic bis (ether amine) s bearing pendent trifluoromethyl groups.* Polymer, 2005. **46**(15): p. 5797-5807.

62. Ghosh, M., *Polyimides: fundamentals and applications*. 1996: CRC Press.

63. Morton-Jones, G., *Polymer processing*. 1989: Springer.

64. Kwon, J., et al., *Fabrication of polyimide composite films based on carbon black for high-temperature resistance.* Polymer Composites, 2014. **35**(11): p. 2214-2220.

65. Foulger, S.H., *Reduced percolation thresholds of immiscible conductive blends.* Journal of Polymer Science Part B: Polymer Physics, 1999. **37**(15): p. 1899-1910.

66. So, H.H., J.W. Cho, and N.G. Sahoo, *Effect of carbon nanotubes on mechanical and electrical properties of polyimide/carbon nanotubes nanocomposites.* European Polymer Journal, 2007. **43**(9): p. 3750-3756.

67. Nayak, L., et al., *Thermal and electrical properties of carbon nanotubes based polysulfone nanocomposites.* Polymer bulletin, 2011. **67**(6): p. 1029.

68. Brigandi, P.J., J.M. Cogen, and R.A. Pearson, *Electrically conductive multiphase polymer blend carbon-based composites.* Polymer Engineering & Science, 2014. **54**(1): p. 1-16.

69. Ioan, S., et al., *Surface and interfacial properties of poly (amic acid) s and polyimides.* Polymer Engineering & Science, 2007. **47**(4): p. 381-389.

70. De, D., et al., *Reinforcing effect of reclaim rubber on natural rubber/polybutadiene rubber blends.* Materials & Design, 2013. **46**: p. 142-150.

71. Ghanbari, A., et al., *Morphology and Gas Barrier Properties of Polymer Nanocomposites.* Polymer Morphology: Principles, Characterization, and Processing, 2016: p. 397-417.

72. Wang, H., et al., *Influence of heat treatment on electromagnetic properties of polyimide/carbon black composites.* Polymers for Advanced Technologies, 2014. **25**(12): p. 1616-1621.

APPENDIX

VITA

Mr. Noppawat Kuengputpong was born in Bangkok, Thailand. He graduated at high school level in 2008 from Joseph Upatham School. He received the Bachelor's Degree of Science with a major in Chemistry from the Faculty of Art and Science, Kasetsart University of, Thailand in 2013. After graduation, he furthers his study for a Master's Degree of Chemical Engineering at the Department of Chemical Engineering, Faculty of Engineering, Chulalongkorn University

Some parts of this work were selected for oral presentations in 1) The 6th International Thai Institute of Chemical Engineering and Applied Science Conference (ITIChE2016) on Innovative Technology toward Sustainable Development which was held during October 26-28, 2016 at Thailand Science Park Convention Center, Bangkok, Thailand and 2) The 7th International Thai Institute of Chemical Engineering and Applied Science Conference (ITIChE2016) on Innovative Technology toward Sustainable Future which was held during October 18-20, 2017 at Shangri-La hotel, Bangkok, Thailand.